茨城大学重点研究

「知的で持続可能な社会基盤および防災セキュリティ技術研究創出事業」

茨城大学工学部附属
防災セキュリティ技術教育研究センター

２０１５年度

報告書

茨城大学重点研究プロジェクト
「知的で持続可能な社会基盤および防災セキュリティ技術創出事業」

平成 27 年度報告書刊行にあたって

プロジェクト代表　　呉　智深

本研究課題は，平成 23 年 4 月に課題募集プロポーザルとその審査により茨城大学重点研究課題として認定され，工学部，教育学部および茨城大学センター教員から構成される異分野研究者の集う場として活動が始まりました．本年度は活動 5 年目を迎えることとなりました．

この報告書では，学術誌論文をはじめとする研究成果に加えて，参加メンバーの学術企画の開催や参加，受賞例についても整理しましたが，「防災セキュリティ技術」という学際領域 に類するテーマが示すように，昨年度に引き続き，多種多様な研究活動とその成果を収めてきたことがわかりました。

2015 年を顧みますと，9 月には我々茨城大学が所在する茨城県内で甚大な自然災害が発生しました．「平成 27 年 9 月関東・東北豪雨」に伴う洪水被害です．茨城県西部を流下する鬼怒川が氾濫したことにより，多くの住宅や公共施設，そして耕作地が被害を受け，人命にまで影響が及ぶ事態となりました．大規模な豪雨の影響は，河川・湖沼の氾濫だけに留まらず，広く流域全体としての自然・社会環境への影響もあり，定常時から社会インフラをセンシングしておくことの重要性を再認識する 1 年となりました．今後，本教育研究センターでは，最終年の研究取りまとめに向けて，主として「統合化」をキーワードとした研究展開を進めるプランを持っております．

今後，センターで得られた成果がより多くの社会基盤維持管理の分野で利用または応用展開が進むよう，メンバー一同，努力を続けて行きたいと考えております．

末筆とはなりますが，茨城大学重点研究課題として採択頂き，茨城大学を代表する研究課題の一つとして諸方面の応援と援助を頂きました茨城大学に心から感謝申し上げますとともに，必ずしも十分でなかった研究交流にも関わらず，本誌に示す多大なる研究成果を上げている参加メンバーに心から敬意と謝意を表します．

今後の研究活動への努力をお約束し，関連する皆様に感謝を申し上げますとともに，ここに平成 27 年度の研究成果を報告させて頂きます．

平成 28 年 3 月吉日
プロジェクト代表　　呉　智深

茨城大学工学部附属防災セキュリティ技術教育研究センター　(2015 年度)
プロジェクト参加教員

呉　　智深　　(工学部都市システム工学科・教授・センター長)
齋藤　　修　　(防災セキュリティ教育研究センター・特命教授・副センター長)
鎌田　　賢　　(工学部情報工学科・教授・副センター長)
桑原　祐史　　(広域水圏環境科学教育研究センター・教授・センター幹事)
沼尾　達弥　　(工学部都市システム工学科・教授)
今井　　洋　　(工学部電気電子工学科・教授)
原田　隆郎　　(工学部都市システム工学科・准教授)
横田　浩久　　(工学部電気電子工学科・准教授)
湊　　淳　　(理工学研究科・教授)
武田　茂樹　　(工学部メディア通信工学科・教授)
澁澤　　進　　(工学部情報工学科・教授)
羽渕　裕真　　(工学部情報工学科・教授)
外岡　秀行　　(工学部情報工学科・教授)
車谷　麻緒　　(工学部都市システム工学科・准教授)
石田　智行　　(工学部情報工学科・助教)

－目次－

1.活動概要

防災セキュリティ教育研究センター　平成27年度活動計画・実施結果調書

1．技術・研究開発分野

担当者氏名：呉　智深　　Email：zhishen.wu.prof@vc.ibaraki.ac.jp

・計画名：社会基盤を対象とした維持管理および防災/減災へ向けたセンサ技術・空間情報応用研究
実施予定時期：平成 27 年 4 月 1 日～平成 28 年 3 月 31 日
・防災・環境教育の実施と地域還元のためのツール開発
実施予定時期：平成 27 年 4 月 1 日～平成 28 年 3 月 31 日
・システムとしての防災・減災技術の確立検討（企業・自治体・学術連携）
実施予定時期：平成 27 年 4 月 1 日～平成 28 年 3 月 31 日

1．実施内容：
・センサ技術の開発
光ファイバセンサ・カーボンファイバセンサ・RFID タグ・UAV・防災/気象用センサ
IC タグ（水位・加速度・傾斜・降雨・大気関連）
・センサデータの安定した通信/解析技術の開発と省電力化推進
マルチホップ通信による耐災害メッセージングシステム
津波を受ける構造物の外力評価
・センサ技術の現地実証の推進と課題抽出
超小型衛星を用いた情報利用技術の検討（継続課題）
老朽化したインフラ構造物の災害リスクを考慮した維持管理計画（継続課題）
・UAV を活用した新たな空間情報の防災システムへの活用と超小型衛星との連携
・アウトリーチとしての防災・減災、それらを含む環境教育の実施
・地元企業・学校等との学術連携実現
・他大学・企業・自治体連携での研究資金獲得
・シンポジウム開催（県内・都内）
・自治体との各種連絡会議推進（茨城県・日立市・ひたちなか市等）
・国際共同研究を実施（アメリカ、英国、イタリア、中国、韓国等）
・大型プロジェクトを申請

2．実施体制（注：外部の人も含む）
責任者：呉 智深（センター長）
メンバ：齋藤　修，鎌田　賢，沼尾　達弥，今井　洋，羽淵　裕真，渋沢　進，湊　淳，横田　浩久，原田　隆郎，武田　茂樹，外岡　秀行，桑原　祐史，車谷　麻緒，石田智行
（茨城高専・東北大学・東京大学・青山学院大学の教員の正式参加を調整中）

3．実施における課題：　　特になし.

4．実施結果（年度末に記載）

（結果）
・茨城県・水戸市連携による、内水氾濫監視システムの実証実験推進（H27 年 3 月に設置準備完了。H28 年 4 月以降に機器設置実施予定）

・茨城県との連携によるUAVのダム長寿命化への応用検討（H27年10月に第一回撮影実施）
・茨城県との連携による常陸大宮地区での傾斜計設置。地盤災害への対応検討実証実験（H27年1月より実施）
・茨城県との連携による常陸大宮、引田橋における加速度センサ設置による橋梁長寿命化対応実証実験（H26年6月より継続中）
・株式会社 KSK 構造診断研究所との連携による新潟県、国道18号妙高大橋における光ファイバセンサ設置による橋梁健全性評価手法の実証実験（H27年5月より実施）
・株式会社 KSK 構造診断研究所との連携による川根大橋におけるカーボンファイバセンサ設置による橋梁振動モニタリング実証実験（H27年11月より実施）
・中国の蘇通長江大橋（橋梁管理局と協力）でのインフラ構造物の早期損傷検知実験（H27年11月より実施）

八戸工大：橋梁長寿命化研究での連携
青山学院大学：UAV飛行におけるプロトコル確立研究連携
東京大学・長岡技術大学：橋梁長寿命化についての情報交換会

ひたちなか市立外野小学校・前渡小学校での環境・情報特別授業実施（H27年9月）

宮城県名取市閖上地区のUAVによる震災被害地アーカイブ映像撮影　宮城教育大学との連携
宮城県女川町・石巻市連携による地盤沈下調査（来年度継続）・UAVによる震災アーカイブ映像撮影

日本地球惑星連合(JPGU)2015：セッション「UAVが拓く新しい世界」コンビーナとしてUAVの活用を推進。

茨城県生活環境部・土木学会茨城支部・㈱新星コンサルタント等においてUAV操作指導・安全教育を実施。

常総市水害（９月１０日）のUAVによる調査・記録・分析に協力（国交省委託事業の一環）

「建設フェスタ2014」（2014年11月9日開催）においてUAV技術展示・成果PRを実施

（課題）　特になし

６．その他（参考資料、報告書など）

2. 人材育成

担当者氏名: 呉　智深	Email:　zhishen.wu.prof@vc.ibaraki.ac.jp

1.　計画名・実施予定時期

計画名:「センサシステム開発−情報ネットワーク−データ解析法」に関する授業の学部～社会人への展開

実施予定時期:平成 27 年 4 月 1 日～平成 28 年 3 月 31 日

2.　実施内容:

下記の学内授業実施および学生国際会議企画を行い、研究で得た最新情報を学部学生へフィードバックし、また、社会人ドクターの教育を通じて高度化する.

①学部学生に対する教育

通信理論, ソフトウェア実現, 空間情報工学

②大学院博士前期課程学生に対する教育

構造物の数値解析法, 衛星画像および地理情報の解析法, 社会基盤情報処理特論

③社会人(専門技術者向)に対する教育

土木学会茨城会で行っているイブニングセミナ(地域の技術者対象)に防災・センシング関連で講座を出す

④その他:小中高校への環境。防災教育の提供

3.　実施体制(注:外部の人も含む)

責任者:呉　智深(センター長)

メンバ:鎌田　賢, 齋藤　修, 沼尾　達弥, 今井　洋, 羽淵　裕真, 渋沢　進, 湊　淳, 桑原　祐史, 横田　浩久, 原田　隆郎, 武田　茂樹, 外岡　秀行, 車谷　麻緒, 石田　智行

4.　実施における課題:　　特になし

5.　実施結果(年度末に記載)

(結果)

・茨城県「いばらき近未来実証推進事業」プロジェクト推進委員会委員（アドバイザー）として、UAV を含むロボット実証試験に安全管理・実証方法についてアドバイスを行っている（齋藤、桑原、鎌田)。

(課題)　特になし

6. その他(参考資料、報告書など)

3. 資金獲得

担当者氏名: 呉　智深	Email:zhishen.wu.prof@vc.ibaraki.ac.jp

1. 計画名・実施予定時期

- 計画名:大型プロジェクトの獲得
- 実施予定時期:平成 27 年 4 月 1 日～平成 28 年 3 月 31 日

2. 実施内容:

科研費はセンターメンバー個々人がチャレンジすることとし，それ以外の大型プロジェクト(国土交通省，経済産業省，総務省)に，共同研究等で関係のある産官学学外機関との連携を取り，チャレンジする.
昨年度に不採択となった概算要求書をベースとして生かす。

3. 実施体制(注:外部の人も含む)

責任者:呉 智深(センター長)
メンバ:鎌田 賢，齋藤 修，沼尾 達弥，今井 洋，羽淵 裕真，渋沢 進，湊 淳，桑原 祐史，横田 浩久，原田 隆郎，武田 茂樹，外岡 秀行，車谷 麻緒，石田 智行

4. 実施における課題:

大型プロジェクトの申請に関する作業時間をより確保する必要がある。

5. 実施結果(年度末に記載)

(結果)
・平成 26 年度募集 SCAT 研究費助成獲得　青山学院大学戸辺教授との連名「複数異種 UAV 間協調動作プロトコルの開発と広域環境観測への応用」
複数の UAV を協調動作させる。防災への応用が期待できる。(H27 年度から 3 年)

(課題)　特になし

6. その他(参考資料、報告書など)

2.研究報告

（H27 年度参加教員発表の代表的な学術論文集）

Experimental Study on Cyclic Response of Concrete Bridge Columns Reinforced by Steel and Basalt FRP Reinforcements

Arafa M. A. Ibrahim[1]; Zhishen Wu, M.ASCE[2]; Mohamed F. M. Fahmy, Ph.D.[3]; and Doaa Kamal[4]

Abstract: This paper presents the seismic performance of concrete bridge columns reinforced with both steel and fiber-reinforced polymer (FRP). A bond-based parametric experimental study was conducted on five FRP steel–reinforced concrete (FSRC) bridge columns—using basalt FRP (BFRP) bars and BFRP sheets—and two steel-reinforced concrete (SRC) bridge columns served as references to investigate the fundamental characteristics of the proposed reinforcement. The investigated bond parameters included the texture of the FRP bars (smooth and ribbed), diameter of the FRP bars, location of the FRP bars with respect to the steel bars, and application of external FRP confinement. All columns were tested under the combined effect of constant axial load and reversed cyclic loading. The experimental results showed that the FSRC bridge column could realize the existence of a stable postyield stiffness (hardening behavior) as well as a reasonable displacement ductility of up to 10 before encountering strength degradation. Moreover, the FRP bars added for column longitudinal reinforcement did not have a substantial impact on the column elastic stiffness. The bond condition of the FRP bars to the surrounding concrete had pronounced effects on the column failure mode, postyield stiffness, residual displacement, and ductility; thus, it could be adopted as a design parameter.
DOI: 10.1061/(ASCE)CC.1943-5614.0000614.

Author keywords: Basalt fiber-reinforced polymer (FRP); Bridge column; Ductility; Damage control; Bond; Postyield stiffness.

Introduction

Ductility, energy dissipation, and strength demand are important seismic performance indices in seismic design of modern concrete bridge columns (Kawashima et al. 1998). In addition, seismic performance of bridges during and after an earthquake is considerably dependent on the importance level of the bridge. For instance, columns of essential bridges should open quickly to all traffic (quickly come back to the original function) after a massive earthquake (AASHTO 2011). Several studies such as Christopoulos et al. (2003) and Pettinga et al. (2007) addressed the importance of the existence of structure postyield stiffness, i.e., ability of structure to continue carrying load after yielding. Actually, the existence of postyield stiffness was considered a seismic performance index (Christopoulos and Pampanin 2004) because the structure residual inclination (permanent deformation) and damage level are dependent on the slope of the postyield stiffness. Other studies (e.g., Priestley et al. 1996; Wu et al. 2009) emphasized that the uncontrollable damage of conventional steel-reinforced concrete (SRC) structures results from the elastoplastic characteristics of ordinary steel bars. To guarantee the existence of postyield stiffness and control damage of a structure, Pettinga et al. (2007) suggested coupling the main structural system with a more flexible secondary system, in which the secondary system is designed to undergo elastic deformations while the main system undergoes inelastic deformations.

During the last two decades, several experimental and analytical investigations have been conducted with the aim of control of the postyield stiffness and mitigation of the postearthquake damage and residual displacement of concrete bridge columns. In this direction, Iemura et al. (2006) incorporated unbonded high-strength tendons in bridge piers to realize a structure with stable postyield stiffness. To enhance the self-centering capability (i.e., the ability of the structure to return to its original configuration after seismic events) of bridge piers, Sakai et al. (2006) and Zatar and Mutsuyoshi (2002) used posttensioned tendons. To avoid the need for mechanical anchors, Davis et al. (2012) used unbonded pretensioned strands. Other studies (e.g., Trono et al. 2015; Dawood et al. 2012; ElGawady and Sha'lan 2011; Chou and Chen 2006) realized the self-centering of concrete bridge piers by adopting posttensioned segmental systems. However, this system has a low energy dissipation capacity compared with conventional monolithic columns (Nikbakht et al. 2013). Therefore, studies by ElGawady and Sha'lan (2011), Marriott et al. (2009), Currie et al. (2009), and others supplied the system with internal and/or external energy dissipaters.

Saiidi and Wang (2006), Saiidi et al. (2009), and Tazarv and Saiidi (2013) used shape memory alloy as longitudinal reinforcement of concrete bridge columns to mitigate residual displacement and plastic hinge damage. However, the high cost, lack of clear understanding of thermomechanical processing, and difficulty in machining of shape memory alloys would bar its expanded use (Desroches and Smith 2003; Varela and Saiidi 2014).

[1]Ph.D. Candidate, Dept. of Urban and Civil Engineering, Ibaraki Univ., 4-12-1 Nakanarusawa-cho, Hitachi 316-8511, Japan. E-mail: arafamai2015@gmail.com

[2]Professor, Dept. of Urban and Civil Engineering, Ibaraki Univ., 4-12-1 Nakanarusawa-cho, Hitachi 316-8511, Japan (corresponding author). E-mail: zswu@mx.ibaraki.ac.jp

[3]Research Fellow, International Institute for Urban Systems Engineering, Southeast Univ., Nanjing 210096, China; and Lecturer, Dept. of Civil Engineering, Faculty of Engineering, Assiut Univ., Assiut 71516, Egypt. E-mail: mfmf1976@yahoo.com

[4]M.Sc. Candidate, Dept. of Urban and Civil Engineering, Ibaraki Univ., 4-12-1 Nakanarusawa-cho, Hitachi 316-8511, Japan. E-mail: 14nm826a@vc.ibaraki.ac.jp

Note. This manuscript was submitted on February 21, 2015; approved on July 6, 2015; published online on October 1, 2015. Discussion period open until March 1, 2016; separate discussions must be submitted for individual papers. This paper is part of the ***Journal of Composites for Construction***, © ASCE, ISSN 1090-0268/04015062(19)/$25.00.

In recent years, numerous research findings evidenced the success of external confinement of concrete columns using fiber-reinforced polymer (FRP) jackets to improve shear, bond, and ductile behavior of concrete columns (Seible et al. 1997; Xiao et al. 1999; Hamad et al. 2004; Haroun and Elsanadedy 2005; Wu et al. 2006; Choi et al. 2013). Zhu et al. (2006) encased a single-segment posttensioned column in a concrete-filled FRP polymer tube to enhance its ductility, and ElGawady et al. (2010) used the same procedure for segmental concrete columns. The columns reached high drift levels with no strength degradation. Despite the effectiveness of FRP confinement to increase the concrete compression strength and restrain the lateral expansions on the core concrete, Fahmy et al. (2010a) concluded that concrete confinement is not the technique that directly controls the column postyield stiffness and residual displacement.

Wu et al. (2009, 2010a) proposed a steel-FRP composite bar (SFCB) as a technique that can be applied in the field of civil engineering to combine the advantageous mechanical and physical properties of both steel and FRP composites. By reinforcing RC bridge columns with SFCB, it would be suitable to control their postyield stiffness and residual displacement. Furthermore, the postyield stiffness depended on the properties of the fibers used, whereby columns reinforced with steel-basalt fiber composite bars exhibited a larger drift capacity before the rupture of the basalt fibers than those reinforced with steel–carbon fiber composite bars (Fahmy et al. 2010b). Although scale model columns reinforced with this type of composite bars exhibit a favorable seismic performance with damage-controllable states after yielding, the production of comparable composite bars for practical application with larger inner steel cores may require an excessive amount of outer longitudinal fiber material, which would complicate the production process; thus, using many composite bars with a smaller inner steel core would be necessary. In addition, the bond performance between composite bars and concrete must be further improved.

Figs. 1(a and b) present the schematic reinforcement of two conventional SRC structures; namely SRC1 and SRC2. Design of SRC1 and SRC2 was assumed to satisfy the strength demands by moderate and strong earthquake, respectively. Therefore, additional increase in the concrete dimensions and/or steel reinforcement is necessary in SRC2, comparing with that of SRC1. This paper proposes coupling the system of the SRC1 with additional FRP reinforcement [Fig. 1(c)]. Fig. 2 presents a detailed mechanical model of the expected performance of the proposed FRP-steel reinforced concrete (FSRC) system in comparison with the two SRC systems. This model is a modified form of the proposed behavior of FRP-RC damage-controllable structure defined by Fahmy et al. (2009), in which further developments meeting the requirements of modern codes for new structures are considered. The FSRC system is proposed for the life safety performance objective because the structure would be able to withstand moderate earthquakes with elastic performance, and the demand strength by strong earthquake could be ensured by the existence of a stable postyield stiffness, K_2 (Fig. 2). Prior to yielding of steel reinforcement, FSRC exhibits initial elastic stiffness, K_1, similar to that of SRC1, but less than that of SRC2. Comparing with SRC systems, FSRC system is characterized by a stability zone of the peak strength, along the line M-S [zero stiffness (K_3)], whereby the structure system demonstrates a desirable ductile performance before degradation of strength. Failure of the FSRC system is defined when the contribution of FRP bars to the lateral resistance is completely lost (at point F). From the viewpoint of postearthquake recoverability, because the FSRC structure contains elastic members and has positive postyield stiffness, both damage level and residual deformations could be controlled.

Recently, basalt FRPs (BFRPs) have emerged as a promising alternative to conventional FRPs in reinforcing concrete structures (El Refai et al. 2015). BFRPs show advantageous characteristics in mechanical, chemical, and high ratio of performance to cost in comparison to other FRPs. For instance, BFRP has a higher strength and modulus, a similar cost, and more chemical stability compared with E-glass FRP; a wider range of working temperatures and much lower cost than carbon FRP (CFRP); and greater than five times the strength and approximately one-third the density of commonly used low-carbon steel bars (Wu et al. 2010b; Sim et al. 2005; Palmieri et al. 2009). Because of the aforementioned characteristics, BFRP was nominated for application in the FSRC system in this study.

Research Significance

To control postyield performance of concrete bridge columns, this study proposed combining steel and FRP reinforcement for concrete structures. Bond between FRP bars and the surrounding concrete was adopted as a key parameter that affects the structural behavior of the proposed column. The objectives of this research were threefold: (1) assessing the cyclic response of RC bridge columns reinforced by steel and FRP reinforcements; (2) examining

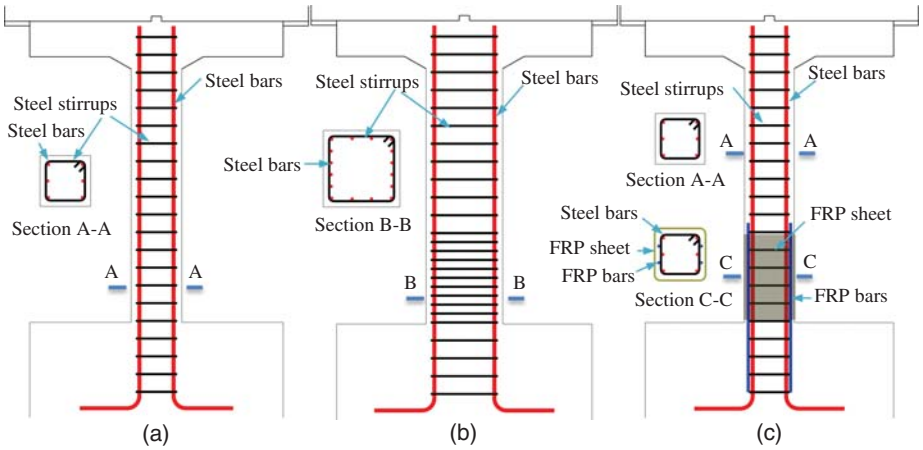

Fig. 1. Schematic reinforcement: (a) SRC1 structure; (b) SRC2 structure; (c) proposed FSRC structure

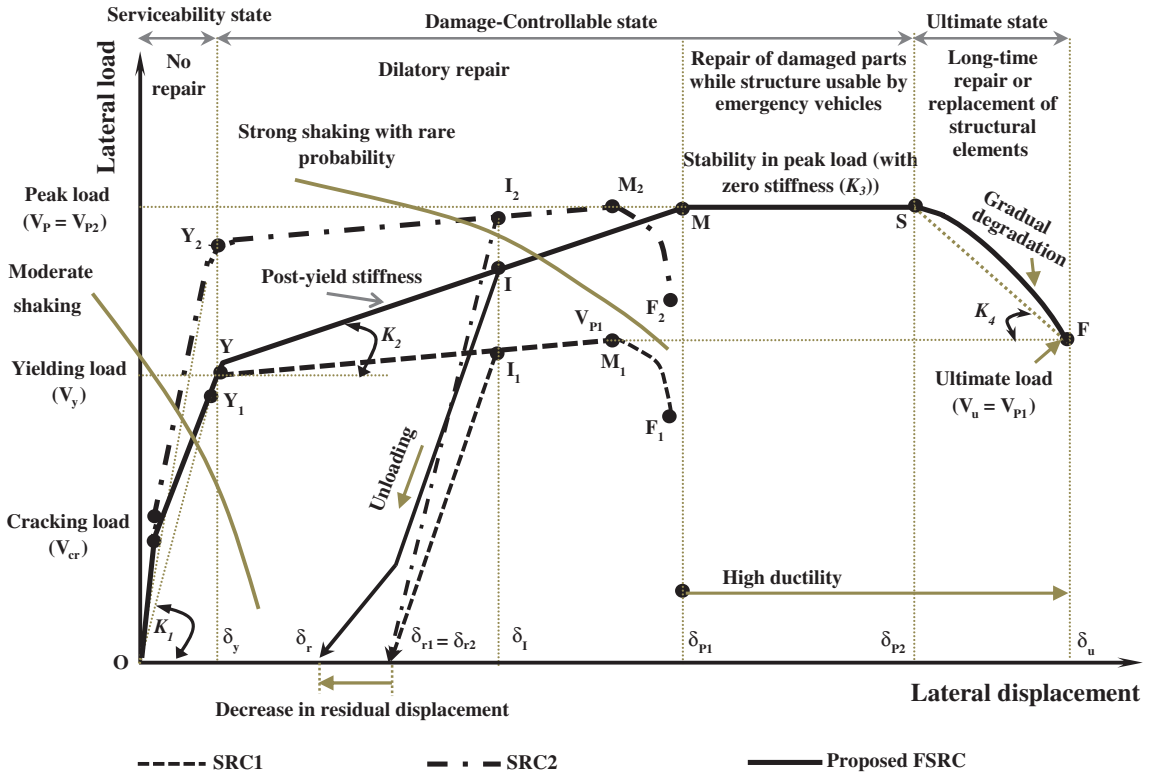

Fig. 2. Targeted idealized load deformation behavior of the proposed FSRC column versus SRC columns

the effect of bond conditions between FRP bars and concrete on the structural performance of the proposed column; and (3) investigating replacement of some steel confinement reinforcement with external FRP jacket. To achieve these objectives, a total of seven one-sixth scale columns were constructed and tested under the effect of combined constant axial load and reversed cyclic load.

Experimental Program

An experimental investigation on concrete bridge columns reinforced with both FRP and steel reinforcement was conducted. One column (CS-4%) was designed as a reference for an RC bridge column that can safely resist strong earthquakes, and another column (CS-2%) was considered to resist nearly half the lateral force of the first column. A complete design was also provided for an FSRC concrete column with the same concrete parameters and steel reinforcement of CS-2% in addition to FRP reinforcement. The subsequent section describes the design parameters of both the steel and FRP reinforcements.

Design of Column Specimens

General Design Parameters

A cantilever bridge column with an overall height of 1.0 m, a cross section of 200 × 200 mm, and a distance from the column base to the point of the lateral load application of 850 mm, yielding an aspect ratio of 4.25, was proposed for this experimental study. These dimensions approximately represent a one-sixth scale of a typical bridge column and were selected based on the available facility capacity of the laboratory, where the tests were carried out. A target compressive strength (f'_c) of 30 MPa was applied to all examined columns. The yield strength (f_y) and ultimate strength of the 13-mm-diameter deformed steel bars used as longitudinal reinforcements were 375 and 560 MPa, respectively; and the corresponding values for the 6-mm-diameter steel transverse reinforcements were 400 and 625 MPa, respectively (Table 1). BFRP bars and BFRP sheet with the mechanical material properties shown in Table 1 were used to investigate the proposed FSRC design. Before applying the proposed cyclic loading that will be explained later, an axial load was applied on all column specimens. Typically, the axial load owing to the superstructure dead weight in bridge columns varies between 5 and 10% of the capacity of the columns. However, in the study of Park (1996), the weight of the bridge superstructure was estimated from the dimensions of the superstructure and columns to cause an axial compression load ratio at the bottom of column specimens of approximately 3%. Other laboratory studies (e.g., Kawashima et al. 1998; Zatar and Mutsuyoshi 2002) assumed an axial compression stress of 1 Mpa to represent the dead weight

Table 1. Mechanical Properties of Steel and FRP Materials

Material type	Elastic modulus E (GPa)	Yield stress f_y (MPa)	Tensile strength f_u (MPa)
Longitudinal steel bars	200	375	560
Transverse steel bars	200	400	625
10-mm-diameter BFRP bars	48.1	—	1,113
8-mm-diameter BFRP bars	47.3	—	1,086
BFRP sheet	91	—	2,100

Note: Tensile strengths of the BFRP bars were defined based on the cross-sectional area of each bar and based on the manufacturer, the basalt fiber content was 60% of the cross-sectional area.

of a highway bridge's superstructure in Japan. Therefore, in this study, a constant axial load of approximately 40 kN (corresponding to 3.3% of the nominal capacity of the column) was applied to each column specimen, inducing an axial compression stress of 1 MPa. Using the aforementioned data, a detailed design of the tested specimens is described next.

Longitudinal Reinforcement

AASHTO (2012) specifies that the area of the longitudinal reinforcement (A_l) of columns located in a high-seismic-hazard area is to be no less than 0.01 or more than 0.04 times the gross cross-sectional area A_g (i.e., $0.01 \le \rho_l \le 0.04$, where ρ_l is the steel reinforcement ratio and equal to A_l/A_g). In this study, the first steel-reinforced column (CS-4%) was reinforced with 12 steel bars of 13-mm diameter (i.e., $\rho_l = \rho_{l\max} = 4\%$, where $\rho_{l\max}$ is the maximum steel reinforcement ratio), whereas the second column (CS-2%) used six longitudinal steel bars of 13-mm diameter (i.e., $\rho_l = 2\%$). The theoretical lateral strengths of these two samples were 67.0 and 36 kN, respectively, and both values were defined using the AASHTO (2012) rectangular stress block for concrete in compression, which has a mean stress of $0.85f'_c$, an ultimate concrete compression strain of 0.003, and a steel stress of f_y for the longitudinal steel bars. The FSRC column was designed to have the same steel reinforcement as column CS-2%, as stated previously. For this column, to reach a strength comparable to that of column CS-4%, additional FRP bars were added. Assuming full contribution of the used BFRP bars (i.e., design strain equals the ultimate tensile strain), four BFRP bars of 10-mm diameter or six BFRP bars of 8-mm diameter would theoretically increase the column strength to the desired value. By summing the area of steel and BFRP bars, the resultant longitudinal reinforcement ratio, ρ_l, became 2.8%. To prevent problems of plastic hinge relocation, anchorage failure, or other failure modes, the BFRP bars in this study were extended to a height of 700 mm from the column base and embedded in the column footing to a depth of 300 mm.

Transverse Reinforcement

In this experimental program, the amount of transverse reinforcement was controlled by the following requirements: (1) confine the plastic hinge regions and prevent early buckling of the longitudinal reinforcement; (2) provide sufficient shear strength; and (3) prevent buckling of FRP bars and improve their bond behavior. To guarantee the aforementioned requirements, the transverse reinforcements in the form of internal steel stirrups and external FRP wrapping were designed as described next.

According to AASHTO (2012), 6-mm-diameter steel stirrups with a spacing of 25 mm should be provided to the plastic hinge region of the columns. Because this amount of transverse reinforcement is independent on the demanded ductility and may result in congestion of reinforcing cages and create concreting problems, 50% of the inner transverse steel reinforcement was replaced with an external FRP jacket. Based on analytical and experimental results, Wehbe et al. (1999) proposed a design expression relating the amount of confining reinforcement to attainable displacement ductility as shown in the following:

$$A_{sh} = 0.1\mu_\Delta \sqrt{\frac{f_{cn}}{f'_c}} S_h h_c \left[0.12\frac{f'_c}{f_{yh}}\left(0.5 + 1.25\frac{P}{f'_c A_g}\right) + 0.13\left(\rho_l \frac{f_{yl}}{f_{sn}} - 0.01\right)\right] \quad (1)$$

where A_{sh} = area of transverse reinforcement in each of the transverse directions; h_c = dimension of the concrete core of the section measured perpendicular to the direction of the hoop bars to the outside of the perimeter hoop; S_h = center-to-center vertical spacing of the hoops; A_g = gross area of the column cross section; $f_{cn} = 27.6$ MPa; $f_{sn} = 414$ MPa; f_{yl} = yield stress of longitudinal steel reinforcement; f'_c = concrete compressive strength; P = axial load; and $\mu\Delta$ = displacement ductility factor.

According to Eq. (1) and using transverse reinforcement of 6-mm-diameter stirrups with a spacing of 50 mm, the resultant $\mu\Delta$ was approximately 8. Referring to the relationship between the curvature and displacement ductility factors of Park and Paulay (1975) and using a reasonable value of the expected plastic hinge length (L_p), the equivalent curvature ductility, μ_ϕ, of approximately 11 could be obtained. To determine the length of the plastic hinge region, Eq. (2) proposed by Paulay and Priestley (1992) was firstly investigated to give a length of 175 mm

$$L_P = 0.08L + 0.022 f_{yl} d_b \quad (2)$$

where L = height of the column to contra-flexure point; and d_b and f_{yl} = diameter and yield stress of longitudinal bars, respectively. However, it was reported by Sheikh and Khoury (1997) that L_p is approximately equal to the cross section size of the confined concrete columns. Therefore, the value of L_p was assumed to be 200 mm.

To determine the required thickness of the BFRP jacket in the plastic hinge region, the demanded ductility for the proposed structure was first identified based on the available literature. Sheikh and Khoury (1997) suggested values of $\mu_\phi \ge 16$, $16 \ge \mu_\phi \ge 8$, and $\mu_\phi \le 8$ for concrete columns with high ductility, moderate ductility, and low ductility, respectively. The New Zealand Society for Earthquake Engineering (NZSEE 2006) recommended values of $\mu_\phi \ge 20$ and $\mu_\phi \ge 10$ for ductile and limited ductile columns, respectively. Wehbe et al. (1999) used values for $\mu\Delta \ge 10$ for high levels of ductility. In this study, to assess the structural performance of the proposed FSRC columns up to high levels of ductility, a value of $\mu_\phi = 20$ ($\mu\Delta > 10$) was assumed. Consequently, a BFRP jacket should be applied to the plastic hinge of the columns to increase μ_ϕ by a value equal to 9. Therefore, the developed procedure of Sheikh and Li (2007) [Eq. (3)] was adopted to determine the required external FRP jackets

$$t_F f_{Fu} = \beta f'_c h(1 + 13k_p^5)\frac{\mu_{\phi,\text{in}}^{1.15}}{29} \quad (3)$$

where t_F = total thickness of FRP jacket; f_{Fu} = ultimate tensile strength of FRP jacket; $\beta = 0.25$ for square columns; h = dimension normal to the loading direction of rectangular columns; k_p is the nominal axial load ratio; and $\mu_{\phi,\text{in}} = \mu_\phi - \mu_{\phi,\text{org}}$, in which μ_ϕ and $\mu_{\phi,\text{org}}$ are the curvature ductility factors after and before FRP jacketing, respectively.

Hence, by assuming a material strength reduction factor of the BFRP jacket equal to 0.65 (CSA 2012), wrapping the plastic hinge region of the columns with a 0.666-mm-thick BFRP jacket was sufficient to achieve the demanded ductility.

At high levels of ductility, in the end regions of concrete columns, for small values of axial compression, the contribution of concrete to resist shear forces is very small (AASHTO 2012). Consequently, by providing the columns with only the internal steel stirrups, the shear capacity of the columns was approximately the same as the theoretical flexural strength of the columns with the highest reinforcement ratio. Therefore, to ensure a dominant flexural failure mode, only half of the calculated BFRP jacket thickness, which was required for plastic hinge confinement, was reasonably extended to a length of 1.5 times the cross-section size of the columns (Seible et al. 1995) (i.e., a 0.333-mm-thick BFRP jacket was extended up to 300 mm height above the column base). Outside the end regions, the contributions from both the transverse steel

reinforcement and the concrete to resist shear forces were enough to prevent any expected shear failure. Ultimately, for FSRC columns with BFRP bars placed in the concrete cover, outside of the steel stirrups, the 0.333-mm-thick BFRP jackets were extended up to a height of 600 mm above the column base. However, because the sensitive design of FRP jacketing for bond purposes is out of the scope of the present study and may be the focus of other works, it is not pursued further in this work.

Test Specimens and Experimental Parameters

Seven different column units were tested to meet the objectives of this study. All column units had a deep heavily reinforced concrete base of $1.0 \times 0.5 \times 0.5$ m (length × width × depth), which simulated a rigid foundation for the tested column. To avoid any unexpected local failure at the loading region, the transverse steel reinforcements were spaced at 30 mm in the highest 300-mm portion of the column units. All columns were attached to a strong steel floor using four vertical high-strength steel rods. The geometry and instrumentation of a typical column unit are shown in Fig. 3. A detailed description of the test specimens follows and is supported by Figs. 3–5 and Table 2:

- Specimen CS-2% [Fig. 4(a)] served as a reference specimen for the steel RC columns. In this column, the longitudinal steel reinforcement consisted of six 13-mm-diameter bars (i.e., $\rho_l = 0.02$), and the transverse reinforcement consisted of 6-mm-diameter internal closed stirrups spaced every 50 mm.
- Specimen CS-2%-J [Fig. 4(b)] was reinforced with the same steel reinforcement as specimen CS-2%. In addition, a BFRP jacket with 0.333-mm thickness was applied to the lowest 300 mm of the column (i.e., $L_{j1} = 300$ mm) and another jacket of 0.333-mm thickness was added to only the lowest 200 mm of the column portion (i.e., $L_{j2} = 200$ mm).
- In addition to the steel reinforcement details of column CS-2%, specimen CSF-2.8%-IS-D10 [Fig. 4(c)] was reinforced with two 10-mm-diameter BFRP bars placed on each of the two opposite sides of the column (those with the highest tension/compression) at the same place as the longitudinal steel bars. The surface texture of the BFRP bars contained small prefabricated indentations (factory product) [Fig. 5(b)].
- Specimen CSF-2.8%-IS-D10-J [Fig. 4(d)] was similar to specimen CSF-2.8%-IS-D10 but wrapped at the lowest region with the same BFRP jacketing as in column CS-2%-J.
- Specimen CSF-2.8%-IR-D10-J [Fig. 4(d)] was the same as specimen CSF-2.8%-IS-D10-J, but the surface texture of the BFRP bars was spirally roughened with BFRP strips in two perpendicular directions [Fig. 5(c)].
- Specimen CSF-2.8%-ES-D10-J [Fig. 4(e)] was the same as specimen CSF-2.8%-IS-D10-J, but the BFRP bars were placed outside the steel stirrups, i.e., in the concrete cover. In addition, a BFRP jacket of 0.333-mm thickness was applied first to the lowest 600 mm of the column portion (i.e., $L_{j1} = 600$ mm) and then another jacket of 0.333-mm thickness was added to only the lowest 200 mm of the column portion (i.e., $L_{j2} = 200$ mm).
- Specimen CSF-2.8%-ES-D8-J [Fig. 4(f)] was reinforced with both steel and BFRP reinforcement and wrapped with the BFRP jacketing as in specimen CSF-2.8%-ES-D10-J, but the FRP reinforcement consisted of three 8-mm-diameter BFRP bars placed external to the steel stirrups on each of the two opposite sides of the column (those with the highest tension/compression) in the concrete cover. The surface texture of the BFRP bars contained small indentations [Fig. 5(a)]. The total reinforcement ratio in this column was approximately 2.8% (i.e., $\rho_l = 0.028$).

Loading and Instrumentation

All columns were subjected to a constant axial load of 40 kN and several excursions of lateral cyclic loading using a dynamic actuator with a capacity of 700 kN. The reversed cyclic loading sequence was determined based on the column displacement at the yielding load (Δy), which was numerically defined for the reference column and kept the same for all specimens. The lateral loading sequence

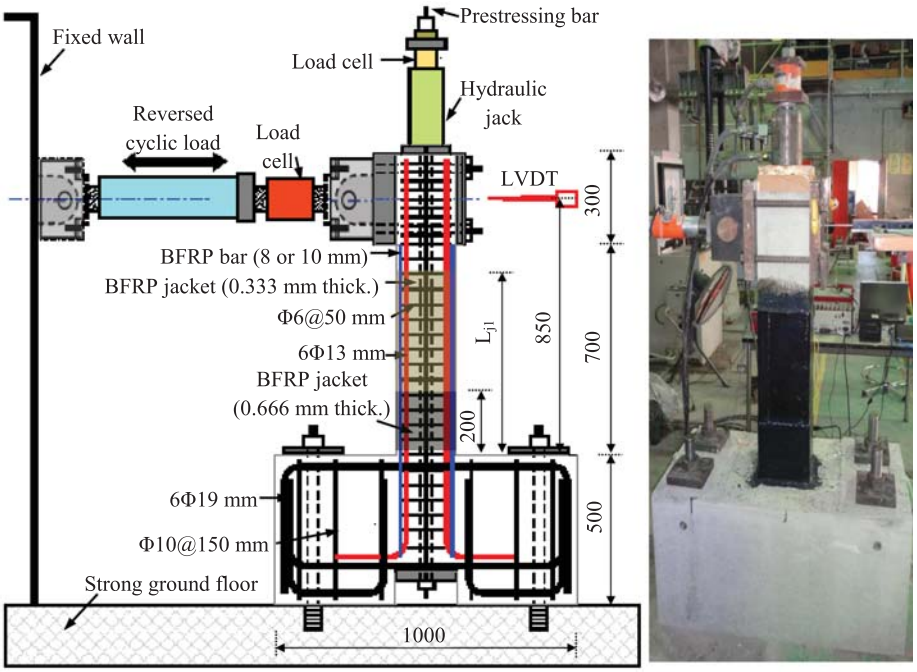

Fig. 3. Typical test unit (dimensions are in mm) and instrumentation of a test specimen

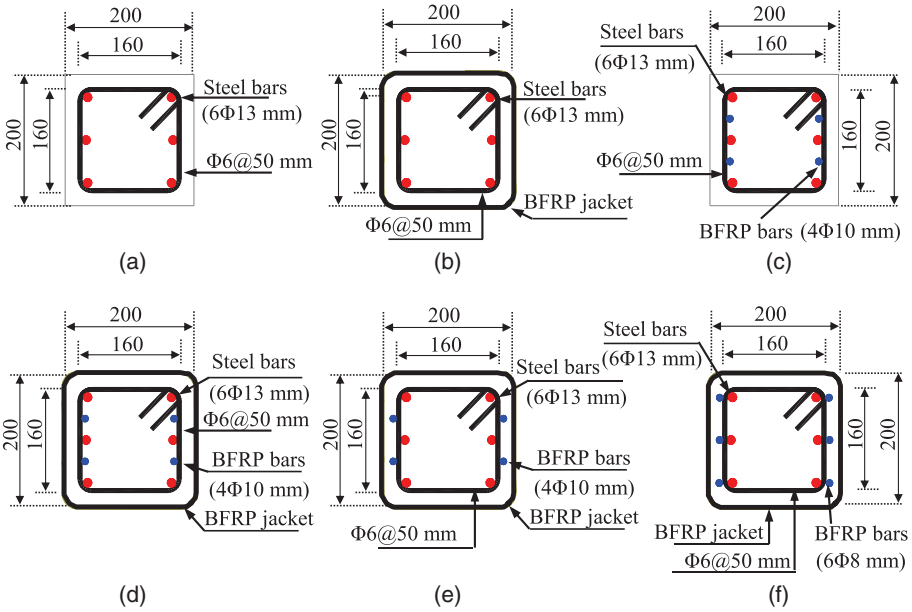

Fig. 4. Cross sections and reinforcement details of specimens (dimensions are in mm): (a) CS-2%; (b) CS-2%-J; (c) CSF-2.8%-IS-D10; (d) CSF-2.8%-IS-D10-J and CSF-2.8%-IR-D10-J; (e) CSF-2.8%-ES-D10-J; (f) CSF-2.8%-ES-D8-J

started with two cycles of $0.5\Delta y$ followed by two cycles of Δy and then three cycles each of $2\Delta y$, $3\Delta y$, $4\Delta y$, $6\Delta y$, $8\Delta y$, and $10\Delta y$ until failure. A linear variable differential transformer (LVDT) was used during testing to record the horizontal displacement of the tested columns. The axial strain histories for both the steel and FRP reinforcements were recorded during the test by using a set of 5-mm-long strain gauges, arranged as shown in Fig. 6. Although efforts were made to keep the axial load constant during the experimental tests, laterally displacing the columns resulted in some variations in the axial load, particularly at high levels of lateral displacement. The actual applied axial load was in the range of 40–100 kN during the tests. All installed instrumentations are shown in Fig. 3.

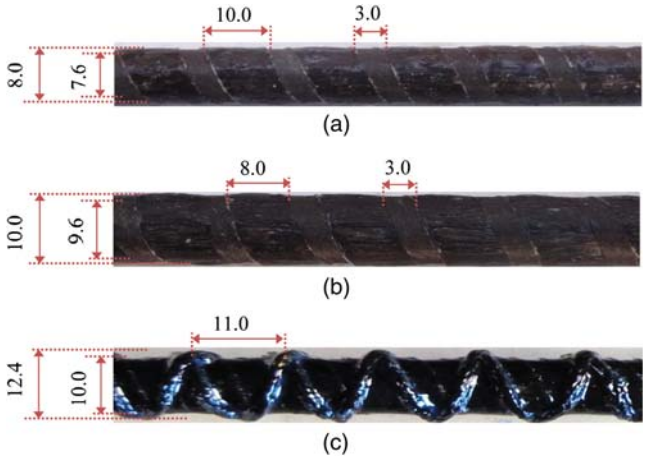

Fig. 5. Configuration of the surface texture of FRP bars: (a) 8-mm-diameter BFRP bar with surface having small indentations (smooth D8); (b) 10-mm-diameter BFRP bar with surface having small indentations (smooth D10); (c) 10-mm-diameter BFRP bar with cross roughened surface (rough D10 bar)

Experimental Results and Discussion

General Observations and Hysteretic Curves

In this section, the results of each column specimen are individually discussed with reference to its hysteretic response (V-δ curve) and failure mode. Fig. 7 shows the lateral load versus the column drift ratio for all tested columns, and Fig. 8 shows the final failure mode of these columns. The deformation capacity of the columns is expressed as the member lateral drift, which is defined as the ratio of the lateral displacement at the point of the load application of each column to the effective height of the column (850 mm). The longitudinal strains of the FRP bars are also examined, where the lateral load-FRP bar strain hysteresis loops were recorded by the FRP bar's strain gauge in each column (Fig. 9). Table 3 summarizes the characteristic values and experimental findings in both the positive and negative loading directions together with the observed failure mode of each specimen, and Table 4 contains the average characteristic values of both directions. The terms V_{cr} and V_y represent the cracking load and steel yielding load, respectively, and the terms δ_{cr} and δ_y represent the corresponding lateral displacements. The cracking load and corresponding displacement were approximately defined from the first turning points of the load-displacement curves when the plastic hinge zone was covered with an FRP jacket. The yielding loads and displacements were obtained from the results of the strain gauges attached to the longitudinal steel bars. The term V_P represents the peak load, and it is characterized by two displacement values δ_{P1} and δ_{P2}, in which δ_{P1} corresponds to the peak load and δ_{P2} corresponds to the end of the plateau zone, if any. The terms V_u and δ_u represent the ultimate load and its corresponding displacement, respectively, and they were defined for SRC specimens at the drift level at which the load capacity decreased to 80% of the peak load. For the other columns (FSRC columns), the ultimate loads and displacements were defined at the degradation of the peak load to the peak load of the SRC column, column CS-2%. Values of the displacement ductility factor, μ, at different characteristic points were superimposed on the hysteretic responses (Figs. 7 and 9), where $\mu = \delta/\delta_y$ and δ = lateral

Table 2. Experimental Parameters

Specimen number	f'_c (MPa)	Steel reinforcement		BFRP reinforcement			ρ_l %	L_{j1} (mm)
		Main	Transverse	Location	Surface	Components		
CS-2%	27.8	6Φ13	Φ6 at 50 mm	—	—	—	2	—
CS-2%-J	31.4	6Φ13	Φ6 at 50 mm	—	—	—	2	300
CSF-2.8%-IS-D10	35.4	6Φ13	Φ6 at 50 mm	Internal	Smooth	4Φ10	2.8	—
CSF-2.8%-IS-D10-J	41.2	6Φ13	Φ6 at 50 mm	Internal	Smooth	4Φ10	2.8	300
CSF-2.8%-IR-D10-J	32.9	6Φ13	Φ6 at 50 mm	Internal	Roughened	4Φ10	2.8	300
CSF-2.8%-ES-D10	32.7	6Φ13	Φ6 at 50 mm	External	Smooth	4Φ10	2.8	600
CSF-2.8%-ES-D8	34.5	6Φ13	Φ6 at 50 mm	External	Smooth	6Φ8	2.8	600

Note: $f_{c'}$ = actual concrete compressive strength on the day of testing; L_{j1} = length of the first 0.333-mm-thick FRP jacket above the column base; ρ_l = total reinforcement ratio of the steel and FRP bars.

displacement at the load application point. Moreover, a complete description of the failures noted during the loading of all columns was included in the hysteretic curves using marked footnotes. The next sections provide a detailed discussion of the behavior of all tested columns.

Columns Reinforced with Steel Bars

For the control specimen CS-2%, flexural cracks first occurred near the column base in the first loading cycle at a drift level of approximately 0.1%, corresponding to a lateral load of 9.2 kN. While displacing the specimen in both loading directions, new horizontal and slightly inclined cracks formed and propagated with further loading and distributed in the lowest 300 mm of the column in both loading directions. The first yielding of the steel bars was observed at a drift level of 0.65%, corresponding to a lateral load of 26.0 kN [Fig. 7(a)]. Afterward, a stable hardening cyclic response appeared and continued up to a drift level of 3.5% ($\mu = 5.3$), corresponding to an average peak load of 37.5 kN in both the push and pull directions. Following this drift level, a peak-loading horizontal plateau was formed with the appearance of significant wide cracks in the plastic hinge regions up to a drift level of 5.9% ($\mu = 8.8$). A bulking of the concrete covers accompanied with a smooth degradation of the cyclic response after this level took place up to a drift level of 7% ($\mu = 10.3$). Beyond this level, a complete spalling and crushing of the concrete cover within a height of approximately 200 mm above the column footing occurred. After the spalling of the concrete cover, a serious buckling of the longitudinal reinforcement [Fig. 8(a)] was observed, causing a sudden drop in the lateral load and terminating the test.

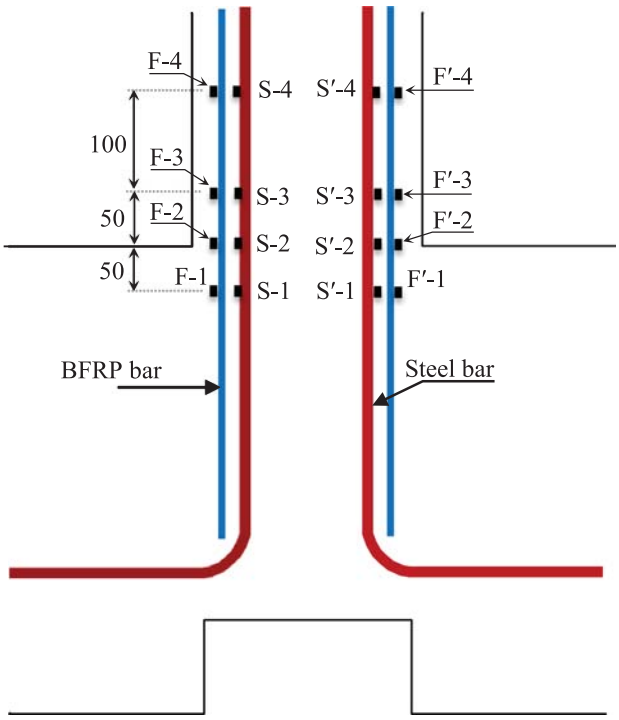

Fig. 6. Typical arrangement of strain gauges

For specimen CS-2%-J, the behavior was significantly affected by wrapping the plastic hinge region with the FRP jacket [Figs. 7(b) and 8(b)]. The use of the BFRP jacket prevented the crack propagation from being observed, but the load-displacement curve demonstrated that the first turning point, indicating the first cracking, was at a drift level and corresponding lateral load nearly the same as those of the control specimen. The first yielding of the steel reinforcement took place at a drift level of 0.64%, corresponding to a lateral load of 27.2 kN (i.e., $V_y = 1.05V_{yc}$, where V_{yc} is the yielding load of column CS-2%). After the yielding of the steel bars, the column was able to continue carrying a load in a stable manner up to a drift level of 5.9% ($\mu = 8.9$), corresponding to a peak lateral load of 43.4 kN (i.e., $V_P = 1.15V_{PC}$, where V_{PC} is the average peak load of column CS-2%). Beyond this drift, a gradual bulging of the FRP jacket accompanied by a smooth gradual loss of strength took place up to an average lateral drift of 9.4% ($\mu = 14.3$), corresponding to a lateral load of 40.8 kN. Upon increasing the lateral displacement beyond this drift level, the bulging of the FRP jacket was accompanied by a local buckling of the steel bars within a height of approximately 100 mm above the column footing, followed by the rupture of some steel bars [Fig. 8(b)].

Columns Reinforced with Both Steel and FRP Reinforcements

Before the yielding of the steel bars, the observed behavior of all FSRC columns was slightly affected by the contribution of the FRP reinforcement. This could be because of the small contribution of the FRP bars to both the column strength and deformation, and this was identified from the average longitudinal strain records of BFRP bars located at both loading sides, which ranged from 8.5 to 11% of the uniaxial rupture strain of the BFRP bars (i.e., $\varepsilon_{fy} = 0.085$ to $0.11\varepsilon_r$, where ε_{fy} is the average strain recorded in the FRP bars at the yielding of the steel bars, and ε_r is the rupture strain of the BFRP bar). This small contribution is owing to the small elastic stiffness ratio between FRP and steel (i.e., $A_f E_f / A_S E_S = 0.095$, where A and E are the gross cross-sectional area and elastic modulus, respectively, and subscripts S and f denote the steel and FRP bars, respectively). Beyond the yielding of the steel bars,

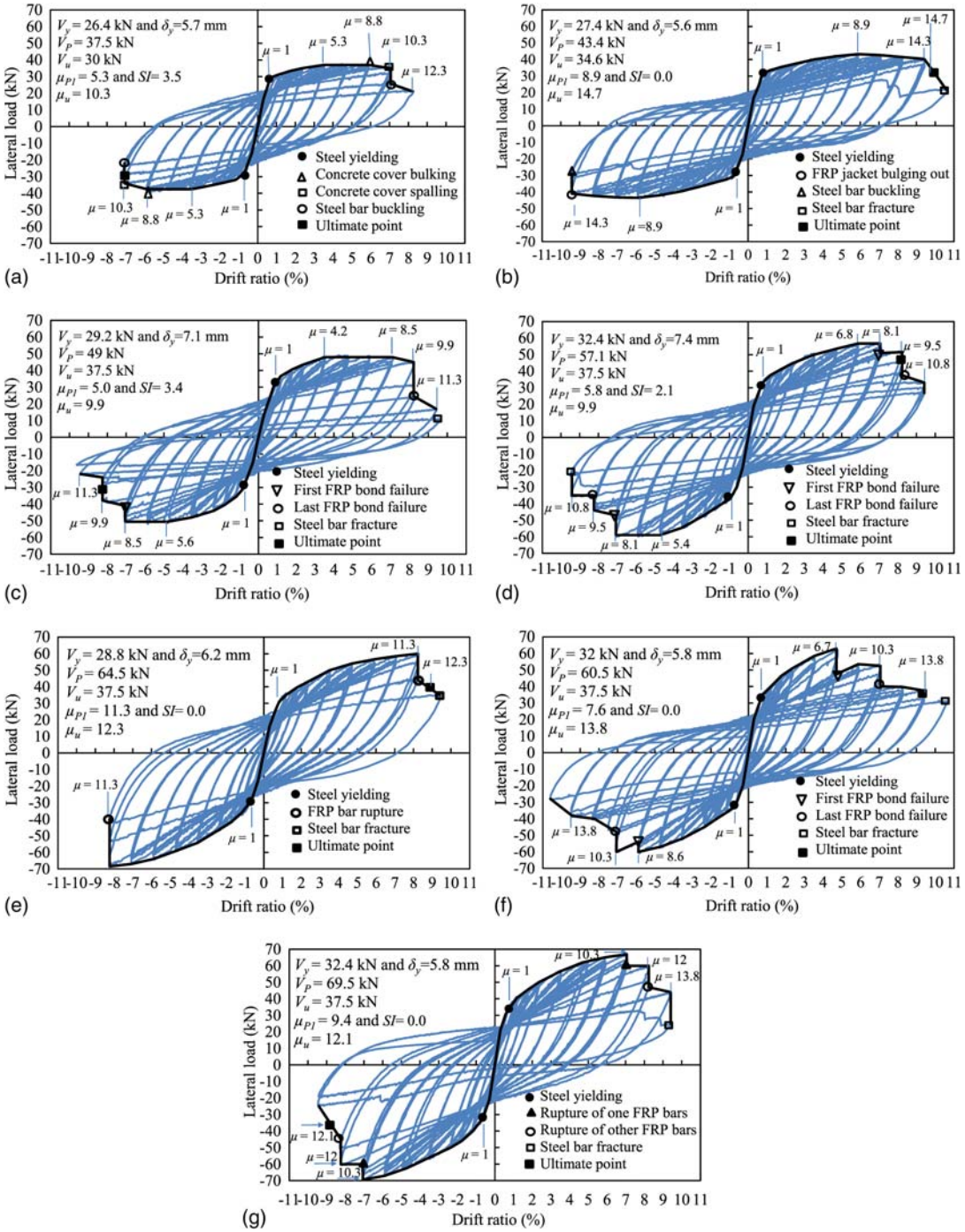

Fig. 7. Load versus drift ratio curves of column specimens: (a) CS-2.0%; (b) CS-2.0%-J; (c) CSF-2.8%-IS-D10; (d) CSF-2.8%-IS-D10-J; (e) CSF-2.8%-IR-D10-J; (f) CSF-2.8%-ES-D10-J; (g) CSF-2.8%-ES-D8-J

the contribution of the FRP reinforcement became significant and controllable, where a hardening zone with a clear positive postyield stiffness was realized. Compared with the control specimen, all specimens reinforced with both steel and FRP bars achieved considerably higher lateral strength (i.e., 30-85% higher than that of column CS-2%). In contrast to the control column, the failure modes of all FRP-reinforced specimens were never attributed to the buckling of the internal reinforcement because a significant portion of the total force in the compression zone was carried by the FRP bars. However, buckling of the longitudinal internal bars occurred abruptly after bond or rupture failure of the FRP bars. The primary observations of the behavior of such columns are subsequently described in detail.

Columns Reinforced with 10-mm-Diameter BFRP Bars

For column CSF-2.8%-IS-D10, small cracks were first observed during the first loading cycle near the column base. With further

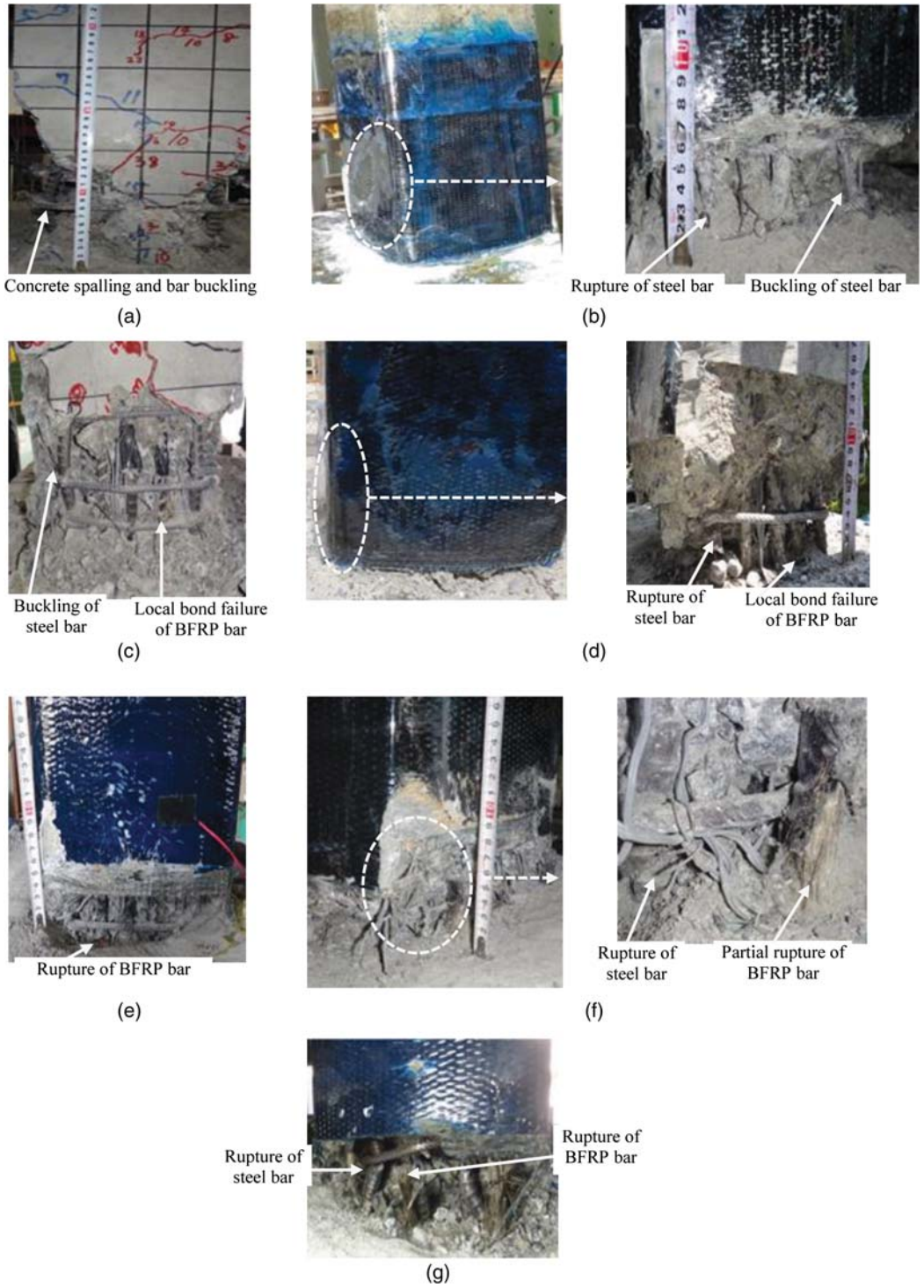

Fig. 8. State of the column specimens at failure: (a) CS-2.0%; (b) CS-2.0%-J; (c) CSF-2.8%-IS-D10; (d) CSF-2.8%-IS-D10-J; (e) CSF-2.8%-IR-D10-J; (f) CSF-2.8%-ES-D10-J; (g) CSF-2.8%-ES-D8-J

loadings, these cracks increased and distributed within the lowest 300 mm of the column height. The applied strain gauges recorded a first yielding strain of the steel bars at a drift level of 0.74%, corresponding to a lateral load of 27.6 kN. Fig. 7(c) shows that beyond the yielding of the steel bars, the column continued carrying loads with a stable postyield stiffness up to a lateral drift of 3.5% ($\mu = 4.2$), corresponding to a peak load of 48 kN ($V_P = 1.28V_{PC}$) in one loading direction. In the other loading direction, a peak lateral load of 50.5 kN ($V_P = 1.35V_{PC}$) was reached at a drift of 4.7% ($\mu = 5.6$). Within this hardening zone, a considerable propagation of cracks appeared and further widened. After reaching the peak load, the concrete cover at the column footing interface and above it started to bulk out, causing a plateau at the peak load level. Along this plateau, concrete crushing and

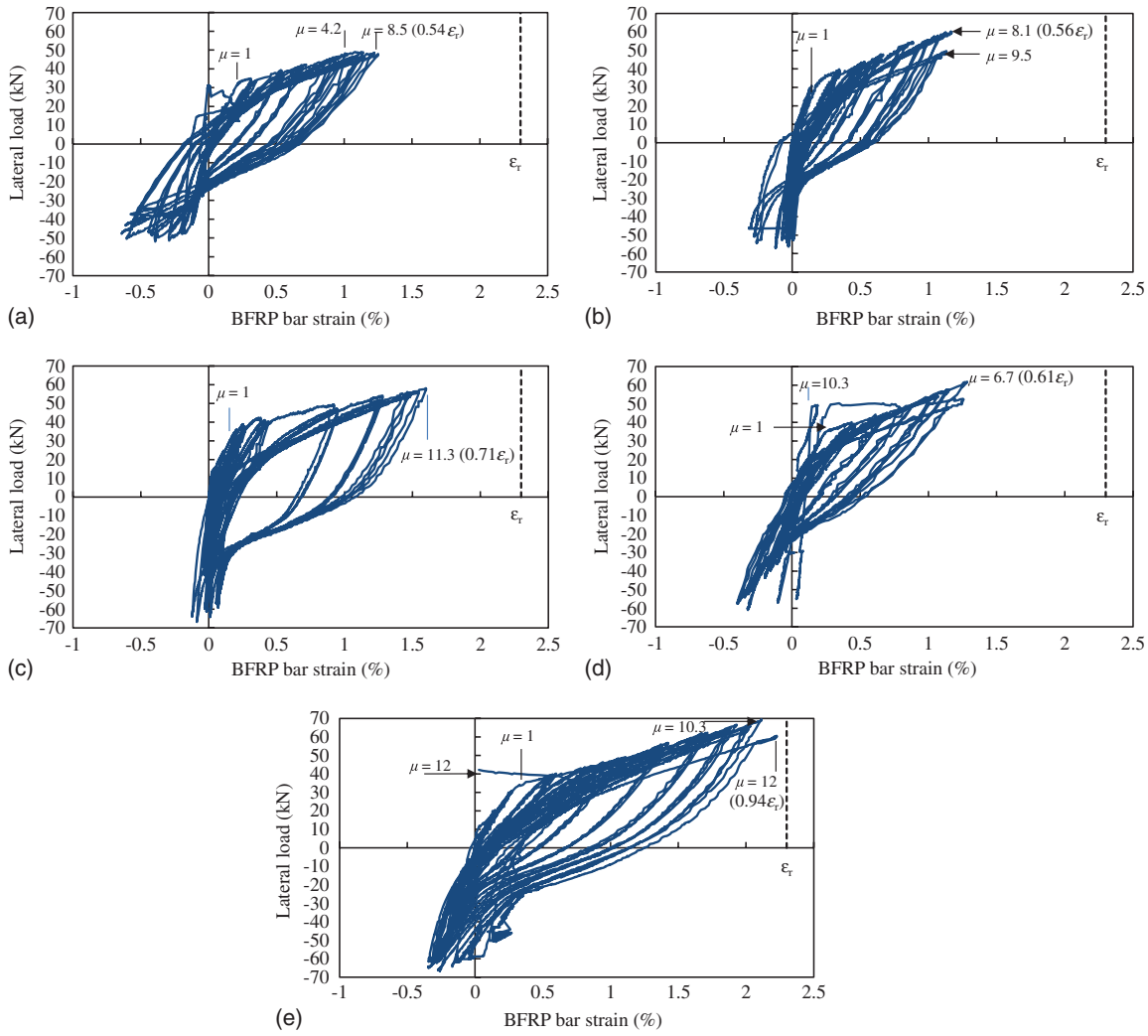

Fig. 9. Load versus BFRP bar strain of FSRC columns: (a) CSF-2.8%-IS-D10 (at 50 mm above column base, F-3); (b) CSF-2.8%-IS-D10-J (at 50 mm above column base, F-3); (c) CSF-2.8%-IR-D10-J (at 150 mm above column base, F-4); (d) CSF-2.8%-ES-D10-J (at 50 mm above column base, F-3); (e) CSF-2.8%-ES-D8-J (at 50 mm above column base, F-3)

spalling became significant, particularly within the first 200 mm near the column footing. A popping sound was heard during the loading of the column to a lateral drift of 7% ($\mu = 8.5$), at which the measured strain ε_f of the BFRP bars was $0.47\varepsilon_r$, indicating the first local bond failure between the FRP bars and surrounding concrete at the column-footing interface. At this drift level, a 20% decrease in the load capacity occurred, confirming the effect of slippage between the FRP bars and surrounding concrete. An additional degradation in the column strength of 5% up to the completion of the first loading cycle to a lateral drift of 8.2% ($\mu = 9.9$) was also observed. A popping sound was heard again when loading to the second and third cycles of the same lateral drift, together with separation of the concrete from the footing, which clearly indicated another local bond failure of the FRP bars. The strain of the FRP bars at this drift level was approximately 54% of the rupture uniaxial strain (i.e., $\varepsilon_{fy} = 0.54\varepsilon_r$) [Fig. 9(a)]. However, as a result of the applied cyclic loading, the partial rupture of the BFRP bars was observed within the first 100 mm above the column base. Consequently, another 40% decrease in the carried load occurred. Hence, all the stresses in the longitudinal direction were carried by the steel bars, resulting in a sudden local buckling of some of them and subsequently their rupture. Fig. 8(c) shows the state of column CSF-2.8%-IS-D10 just before the rupture of the steel bars.

Figs. 7(d), 8(d), and 9(b) show that the observed trim of the behavior of specimen CSF-2.8%-IS-D10-J was similar to that of specimen CSF-2.8%-IS-D10 up to a high loading level. The first yielding of the steel bars was recorded at a lateral load of 28.1 kN, corresponding to a drift of 0.6%. The column achieved a peak load of 56.75 kN ($V_P = 1.51V_{PC}$) at a drift level of 5.9% ($\mu = 6.8$) in one loading direction and a peak load of 59 kN ($V_P = 1.57V_{PC}$) at a drift of 4.7% ($\mu = 5.4$) in the opposite loading direction. Beyond the peak load, a stability in this load was observed up to a drift level of 7% ($\mu = 8.1$), at which point the first bond failure of the FRP bars occurred, causing an average decrease of 15% in the lateral load. Beyond this deformation level, the column maintained the remaining lateral load up to a drift level of 8.2% ($\mu = 9.5$), at which point a complete debonding of the FRP bars occurred, accompanied by another drop in the lateral load by approximately 20%. As a consequence, the steel bars became vulnerable to high stresses, resulting in local buckling and subsequent rupture of some

Table 3. Positive and Negative Characteristic Values of the Hysteretic Curves of the Tested Columns

Specimen number	V_y (kN)	δ_y (mm)	ε_{fy} (%)	V_P (kN)	δ_{P1} (mm)	δ_{P2} (mm)	V_u (kN)	δ_u (mm)	ε_{fu} (%)	Failure mode
CS-2%	+26.0	+5.4	—	+37.3	+30.0	+50.0	+29.8	+58.5	—	Cover spalling and bar buckling
	−26.8	−6.0	—	−37.8	−30.0	−50.1	−30.2	−59.0	—	
CS-2%-J	+27.2	+5.6	—	+43.3	+50.0	+50.0	+34.6	+83.2	—	Fracture of steel bars
	−27.6	−5.5	—	−43.5	−50.0	−50.0	−34.8	−80.0	—	
CSF-2.8%-IS-D10	+30.8	+7.9	+0.20	+48.0	+30.0	+59.9	+37.5	+70.1	+1.09	Local bond slip of FRP bars
	−27.6	−6.3	−0.18	−50.0	−41.3	−59.9	−37.5	−70.1	−1.39	
CSF-2.8%-IS-D10-J	+28.1	+5.3	+0.17	+56.75	+50	+59.1	+37.5	+70.0	+1.22	Local bond slip of FRP bars
	−36.7	−9.6	−0.25	−59	−40.0	−58.7	−37.5	−76.9	−1.32	
CSF-2.8%-IR-D10-J	+29.4	+6.5	+0.20	+60.0	+69.7	+69.7	+37.5	+76.4	—	Rupture of FRP bars
	−28.1	−5.9	−0.22	−69.0	−70.1	−70.1	−37.5	−76.4	−1.63	
CSF-2.8%-ES-D10-J	+33.2	+5.7	+0.23	+61.0	+40.8	+40.8	+37.5	+80.0	—	Local bond slip of FRP bars
	−30.8	−5.8	−0.19	−60.0	−48.0	−50.0	−37.5	−80.0	−1.41	
CSF-2.8%-ES-D8-J	+32.9	+6.0	+0.28	+68.0	+60.0	+60.0	+37.5	+80.0	—	Rupture of FRP bars
	−31.9	−5.6	−0.26	−71.0	−60.0	−60.0	−37.5	−74.9	−2.22	

Note: the symbols "+" and "−" stand for the characteristic values in the positive and negative loading directions, respectively.

Table 4. Average Characteristic Values of the Hysteretic Curves of the Tested Columns

Specimen number	V_{cr} (kN)	δ_{cr} (mm)	V_y (kN)	δ_y (mm)	ε_{fy} (%)	V_P (kN)	δ_{P1} (mm)	δ_{P2} (mm)	V_u (kN)	δ_u (mm)	ε_{fu} (%)
CS-2%	9.2	0.9	26.4	5.7	—	38	30	50	30.0	59	—
CS-2%-J	9.4	1.0	27.4	5.5	—	44	50	50	34.7	82	—
CSF-2.8%-IS-D10	10.0	1.3	29.2	7.1	0.19	49	36	60	37.5	70	1.24
CSF-2.8%-IS-D10-J	10.6	1.2	32.4	7.4	0.21	57	45	59	37.5	73	1.27
CSF-2.8%-IR-D10-J	10.7	1.2	28.8	6.2	0.21	65	70	70	37.5	76	1.63
CSF-2.8%-ES-D10-J	12.6	1.1	32.0	5.8	0.21	61	44	45	37.5	80	1.41
CSF-2.8%-ES-D8-J	12.7	1.0	32.4	5.8	0.27	70	60	60	37.5	76	2.22

of them, causing a termination of the column test [Fig. 8(d)]. The maximum achieved strain in the FRP bars before the bonding failure was approximately 56% of the rupture strain [Fig. 9(b)].

The response of column CSF-2.8%-ES-D10-J shows the effect of placing FRP bars out of the transverse reinforcement in the concrete cover [Fig. 7(f)]. Compared with CSF-2.8%-IS-D10-J that was internally reinforced with FRP bars, a slight increase in the carried lateral load could be achieved. This increase was attributed to the increase in the effective depth of the FRP bars (i.e., the distance from the fibers of the maximum compression strain to the center of the FRP bars located on the tensile side). As shown in Fig. 7(f) and summarized in Table 3, the first yielding of steel bars was recorded at a drift level of 0.67%, corresponding to a lateral load of 33.2 kN. Beyond the yielding of the steel bars, the column showed a gradual increase in the carried lateral load in both loading directions up to drift levels of +4.7% ($\mu = 6.7$) and −5.9% ($\mu = 8.6$), corresponding to lateral loads of +63kN ($V_P = 1.68V_{PC}$) and −60kN ($V_P = 1.6V_{PC}$), respectively. Afterward, local bond failure of the FRP bars occurred as the bond stress between the FRP bars and surrounding concrete reached the bond strength. Two successive drops of the lateral load were observed in both loading directions, where the lateral load in the two loading directions at a drift level of 9.4% ($\mu = 10.3$) reached values of +37.5 and −38.3 kN. Before the debonding of the FRP bars, the recorded strain was approximately 61% of the rupture strain [Fig. 9(d)]. The presence of the FRP bars outside the closed stirrups resulted in a pronounced rupture of the external fibers of the BFRP bars, particularly after the bulging of the BFRP jacket [Fig. 8(f)].

Specimen CSF-2.8%-IR-D10 examined the effect of roughening the texture of the BFRP bars on the bond between the FRP bars and concrete. Fig. 7(e) and Table 3 show that the first yielding of steel bars was at a lateral drift of 0.69%, corresponding to a lateral load of 28.1 kN. Beyond the yielding of the steel bars, a hardening zone of this column was realized in a manner quite similar to that in column CSF-2.8%-IS-D10, with smooth FRP bars, up to a drift level of 3.5%. After this lateral drift ratio, the hysteretic loops showed a continuous increase in column strength but with a smaller positive stiffness in both loading directions up to the completion of the first loading cycle of the lateral drift of 8.2% ($\mu = 11.3$), corresponding to lateral loads in the positive and negative directions of 60 kN ($V_P = 1.6V_{PC}$) and 69 kN ($V_P = 1.84V_{PC}$), respectively. Displacing the column in the two directions with the additional two loading cycles to the same lateral drift resulted in an approximately 25% loss in the achieved peak lateral strength. This drop was primarily attributable to a complete rupture of the FRP bars at 50 mm above the column base [Fig. 8(e)]. At this loading stage, a loud sound was heard, and a bulge formed in the BFRP jacket. During the loading process, the strain gauges located at the section of maximum moment failed early, and only the strain gauge located at 150-mm height continued until the rupture of the BFRP bars. The maximum attained axial strain of the FRP bars recorded by this strain gauge was approximately 71% of the uniaxial rupture strain [Fig. 9(c)]. Following the rupture of the FRP bars, a sudden increase in the stresses were experienced by the steel bars, causing some of them to rupture.

Columns Reinforced with 8-mm-Diameter BFRP Bars

The observed behavior of specimen CSF-2.8%-ES-D8-J was highly similar to that of the column reinforced with rough BFRP bars; this could be attributed to good bond conditions between the FRP bars and surrounding concrete in both cases. As shown in Fig. 7(g) and Table 3, the first yielding of the steel bars was recorded at a drift level of 0.65%, corresponding to a lateral load of 31.9 kN. Beyond the yielding of the steel bars, this column achieved the largest lateral resistance among all tested columns,

where at a drift of 7% ($\mu = 10.3$), the maximum attained lateral strengths in the positive and negative directions were 68 kN ($V_P = 1.81V_{PC}$) and 71 kN ($V_P = 1.89V_{PC}$), respectively. At this drift level, a loud sound was heard, indicating the probability of rupture of one or more FRP bars, followed by an approximately 15% decrease in the peak load. The column was then able to maintain its achieved strength up to a lateral drift of 8.2%, at which point a second loud sound was heard, indicating the probability of rupture of the additional FRP bars, accompanied with another 25% decrease in the lateral load, after the completion of the second loading cycle at this drift level. Unfortunately, the results of the third loading cycle at this drift level were lost during the transfer of the data from the logger. The continued displacement of the column led to a rupture of some steel bars. The results of this column indicated that the FRP bars fulfilled nearly 94% of its rupture strain before failure [Fig. 9(e)]. Moreover, after removing the FRP jacket at the lowest part of the column, the decreases in the lateral load were confirmed to result from the rupture of the FRP bars [Fig. 8(g)].

Envelope Responses

To investigate the effect of each tested parameter individually, the average skeleton curves of push and pull loading directions of all specimens are shown in five separate figures, where the effect of each parameter can be investigated in one figure [Fig. 10]. Referring to Fig. 2, the effectiveness of the proposed column reinforcement should be evaluated in light of the targeted mechanical load-displacement model. To this end, the evaluation process is presented in this section in terms of initial stiffness, postyield stiffness, stiffness degradation, and ductility measurements [Table 5]. To draw firm conclusions, the response of the steel RC column (CS-4%), discussed earlier, was numerically simulated using the *OpenSees* software (Mazzoni et al. 2009). The experimentally applied cyclic loading regime was adopted in the numerical simulation to predict the behavior of column CS-2% for comparison with the experimental results [Fig. 10(a)] and then to predict the performance of column CS-4%. Only the envelope response of the hysteretic curve is presented in this study for comparison with the FSRC columns.

Initial Stiffness

The initial stiffness or elastic stiffness (K_1) is an important seismic performance measure (index) that can be evaluated as $K_1 = V_y/\delta_y$. Higher values of this index would lead to a shorter vibration period of the structure and would generally increase the earthquake forces received (Saiidi et al. 2009). However, as stated by ElGawady and Sha'lan (2011), during a real earthquake scenario, the stiffness reduction is anticipated to lengthen the natural period of vibration of the structure, leading to a potential reduction in the seismic demand forces that is associated with larger displacement demands; therefore, depending on the design approach, there would be a trade-off between the displacement and force demands. K_1 was determined for all tested specimens to investigate the effect of adding FRP reinforcement to the steel reinforcement (Table 5).

As shown in Fig. 10 and summarized in Table 5, adding FRP composites to the steel reinforcement resulted in an insignificant change in the initial stiffness values. Although wrapping the plastic hinge region with an FRP jacket resulted in a significant enhancement in the column confinement, the increase in the initial stiffness was extremely small: K_1 of column CS-2%-J = 1.06; K_1 of column CS-2%, and K_1 of column CSF-2.8%-IS-D10-J = 1.07; and K_1 of column CS-2%-J= 1.06 times that of column CS-2% and K_1 of column CSF-2.8%-IS-D10-J = 1.07 times that of column CSF-2.8%-IS-D10. Placing additional FRP bars at the same place as the steel bars had no clear effect on the initial stiffness compared with the reference column CS-2%, whereas adding FRP bars of 8- or 10-mm diameter in the concrete cover (outside the transverse reinforcement) resulted in an approximately 20% increase in the initial stiffness. Moreover, the bond condition between the FRP bars and concrete showed no considerable effect on the initial stiffness: K_1 of column CSF-2.8%-IR-D10-J $\cong K_1$ of column CSF-2.8%-IS-D10-J; and K_1 of column CSF-2.8%-ES-D8-J $\cong K_1$ of column CSF-2.8%-ES-D10-J. In contrast, Fig. 10(b) and Table 5 show that the initial elastic stiffness of the numerically investigated column CS-4% was more than twice that of the control specimen. That is, increasing the column strength to withstand a strong earthquake using additional steel reinforcement would greatly affect the elastic stiffness and in turn its vibration period, whereas adding FRP bars to an RC structure would be a reasonable solution to avoid any increase in the imposed seismic force on the structure.

Postyield Stiffness

In this section, the postyielding stage of the tested columns up to the column peak strength was evaluated using two postyield stiffness indices. The first index was the ratio between the column postyield stiffness and elastic stiffness ($k = k_2/k_1\%$), where the starting point of the postyield stiffness of all tested columns was defined as the theoretical strength of the control specimen CS-2% defined previously using AASHTO (2012), whereas the endpoint was that corresponding to the maximum achieved lateral strength of the considered specimen (i.e., at a lateral load of V_P and the corresponding lateral displacement δ_{P1}) (Fig. 2). By defining the postyield stiffness using the aforementioned start and endpoints, the curvature in the hardening zone of the load-displacement curves was idealized to a straight line. The second measure was the column displacement ductility, corresponding to the endpoint of the hardening zone (i.e., $\mu_{P1} = \delta_{P1}/\delta_{Py}$). The two indices were calculated for all specimens and are summarized in Table 5. A detailed explanation concerning the efficiency of the proposed FSRC column design to achieve the desired level of lateral strength (the strength of column CS-4% = 67 kN) as well as the effect of the investigated parameters on the postyield stiffness behavior is as described next.

Fig. 10(a) and Table 5 illustrate that control specimen CS-2% continuously increased in lateral strength with the increase in the applied displacement up to a ductility of 5.3 (i.e., $\mu_{P1} = 5.3$). The achieved postyield stiffness ratio corresponding to this final ductility of the hardening zone was 7.8%. Through wrapping the plastic hinge zone with an FRP jacket, as in column CS-2%-J, the column showed an ability to receive a greater lateral load up to μ_{P1} of 9.0, but the postyield stiffness ratio decreased to 6.6%. A substantial decrease in the column postyield stiffness ratio of approximately 52% was observed when increasing the amount of steel reinforcement, as in column CS-4%. In contrast, a significant increase in the postyield stiffness ratio was observed when adding FRP bars (Fig. 10). Fig. 10(b) illustrates that column CSF-2.8%-IS-D10 had a value of k more than twice that of column CS-2%, although the two columns share nearly the same value of μ_{P1}. Changing the location of the FRP bars from the place of the steel fibers (column CSF-2.8%-IS-D10-J) to outside the steel stirrups (in the concrete covers, such as in column CSF-2.8%-ES-D10-J) resulted in a 30% increase in the value of μ_{P1} and a 17% decrease in the value of k [Fig. 10(c)]. Furthermore, by adding cross ribs to the surface of the FRP bars, as in column CSF-2.8%-IR-D10-J, the value of k decreased from 17.3 to 12%, although μ_{P1} shifted from 5.8 to 11.3 [Fig. 10(d)]. This gives a high responsibility to the surface texture of the FRP bars to control the length of the hardening

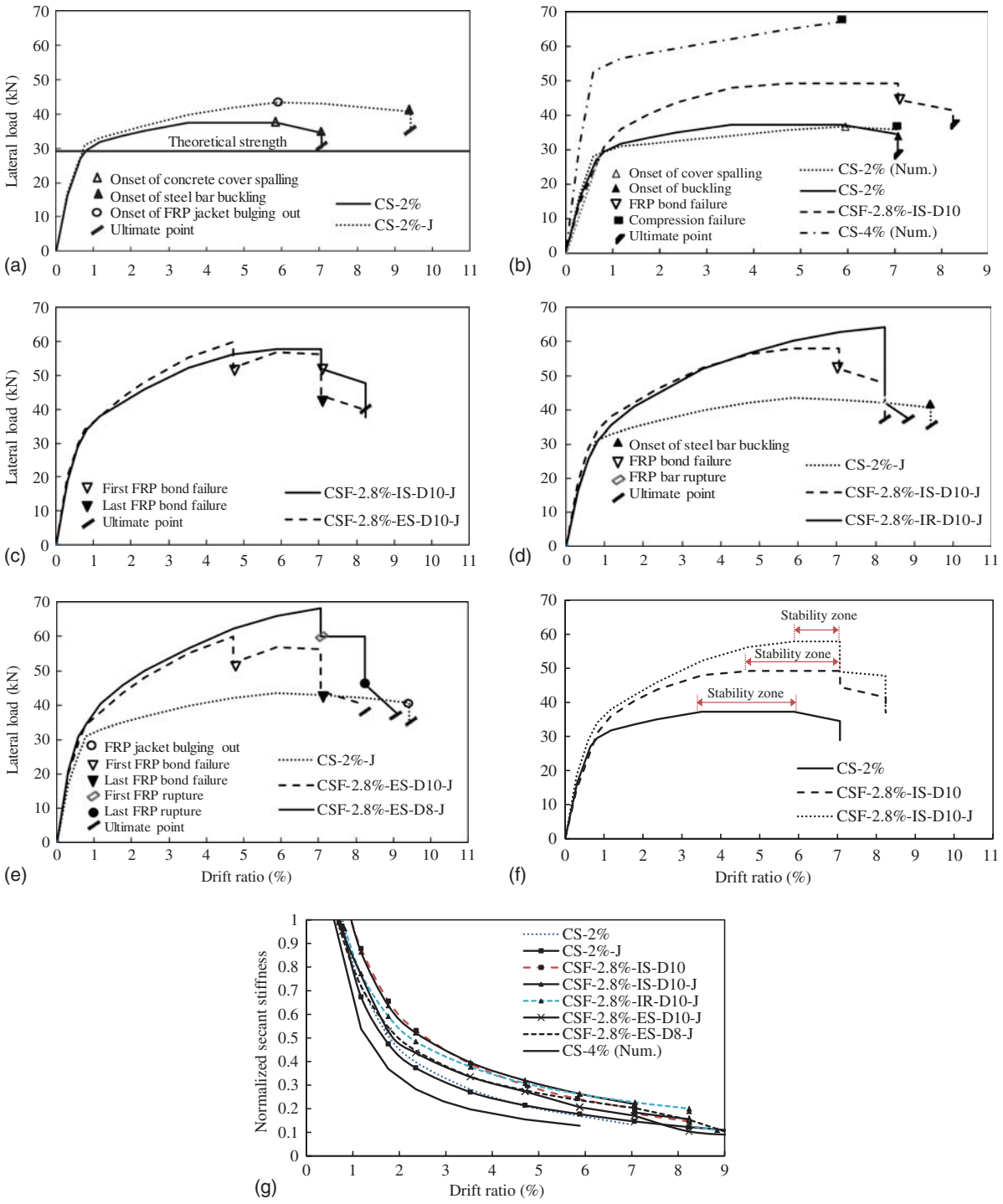

Fig. 10. Effect of the investigated parameters on the backbone curves and stiffness degradation: (a) FRP wrapping; (b) comparison between SRC and FSRC columns; (c) location of FRP bars; (d) FRP bar's surface configuration; (e) FRP bar's diameter; (f) columns contained stability plateau; (g) normalized secant stiffness versus lateral drift ratio

zone. Finally, the postyield stiffness represented by the two indices could be increased by using FRP bars with smaller cross-sectional areas. For instance, columns CSF-2.8%-ES-D10-J and CSF-2.8%-ES-D8-J, with the same FRP-to-steel stiffness ratio, had similar values of k; whereas μ_{P1} shifted from 7.7 to 10.4 when decreasing the diameter to 8 mm. This confirmed the previous observation regarding the ability of the bond conditions of FRP to concrete to control the ductility at the endpoint of the achieved postyield stiffness. The previous discussion demonstrated that by adding FRP bars with a good bonding condition to concrete (8-mm-diameter bars or rough bars), the column could achieve the demanded lateral strength at high ductility levels through a stable postyield stiffness. Compared with these cases, using FRP bars with a weaker bond to concrete resulted in an unfavorable ductility and lateral strength at the end

Table 5. Ductility and Stiffness Indices of the Investigated Columns

	Stiffness indices				Ductility indices		
Specimen number	K_1 (kN/mm)	K_2 (kN/mm)	k (%)	μ_{P1} (mm/mm)	SI (mm/mm)	K_4 (kN/mm)	μ_u (mm/mm)
CS-2%	4.6	0.36	7.8	5.3	3.5	0.86	10.3
CS-2%-J	4.9	0.33	6.6	9.0	0.0	0.27	14.7
CSF-2.8%-IS-D10	4.1	0.69	16.7	5.0	3.4	1.14	9.9
CSF-2.8%-IS-D10-J	4.4	0.76	17.3	5.8	2.1	1.40	9.9
CSF-2.8%-IR-D10-J	4.6	0.56	12.0	11.3	0.0	4.14	12.3
CSF-2.8%-ES-D10-J	5.5	0.80	14.4	7.7	0.0	0.65	13.8
CSF-2.8%-ES-D8-J	5.6	0.73	13.1	10.4	0.0	1.83	13.4
CS-4% (numerical)	10.5	0.40	3.8	10.0	—	—	10.0

of the postyield stiffness; however, it results in a larger postyield stiffness ratio.

Stiffness Degradation

Because of its importance for nonlinear modeling of structures (ElGawady and Sha'lan 2011), stiffness degradation of the tested specimens is compared in this section. Fig. 10(g) shows the normalized secant stiffness [i.e., secant stiffness normalized by the initial stiffness (NSS)] versus the corresponding drift ratios for every specimen. As shown in the figure, the NSS values of the specimen CS-4% at all drift levels were clearly small and its secant stiffness degradation was very fast compared with those of the other specimens. Similarly, the NSS values of the specimens CS-2% and CS-2%-J were smaller and their secant stiffness degradations were faster than those of the FSRC specimens. Among all the FSRC specimens, the secant stiffness of the specimens reinforced with smooth BFRP bars located in the outside of the stirrups degraded faster than others. The reasons for the aforementioned remarks are attributed to the elastic and postyield behavior and the failure modes of the columns, where the steel RC columns were characterized by cover spalling, concrete crushing, and bar buckling before failure. For the FRP-steel columns, the bond behavior of the BFRP bars was the key parameter controlling the stiffness degradation.

Column Ductility

Aside from the displacement ductility corresponding to the endpoint of the postyield stiffness, as explained in the previous section, three other indices were also used in this study to evaluate the ductility behavior and investigate the effect of the tested parameters. The first is the peak strength stability factor, which measures the ability of a structure to undergo large displacements after achieving the peak lateral strength and before entering the degradation zone [i.e., $\mathrm{SI} = (\delta_{P2} - \delta_{P1})/\delta_y$]. The second is the degradation stiffness factor, which defines the ability of a structure to reach its ultimate load through a gradual degradation path [i.e., $K_4 = (V_P - V_u)/(\delta u - \delta_{P2})$]. Through this definition, a smaller value of this index indicates a stable degradation behavior and vice versa. The last ductility measure is the displacement ductility factor at the ultimate lateral strength ($\mu_u = \delta_u/\delta_y$). Referring to the proposed mechanical model (Fig. 2), Table 5 summarizes the ductility indices for all tested columns.

For the control specimen, after reaching its peak lateral load at a μ_{P1} of 5.3, it achieved a stability index of SI = 3.5. This means that the column maintained its peak lateral strength up to a displacement ductility of 8.8 before entering the degradation zone. Following the stability zone, the column reached its ultimate strength at an ultimate displacement ductility, μ_{uC}, of 10.3 through a degradation stiffness factor, K_{4C}, of 0.86.

A significant enhancement in the column ductility could be achieved by wrapping the plastic hinge zone of the steel RC column with an FRP jacket. Although no clear stability zone was formed in column CS-2%-J [i.e., $\mu_{P1} \cong (\mu_{P1} + \mathrm{SI})$ of column CS-2%], the column fulfilled its ultimate strength (i.e., $V_u = 0.8V_P$) at a displacement ductility of 14.7 (i.e., $\mu_u = 1.43\mu_{uC}$) through a degradation factor of 0.27 (i.e., $K_4 = 0.3K_{4C}$). In the absence of the FRP jacket, no pronounced enhancement in the ductility indices could be achieved by adding internal smooth FRP bars to the longitudinal reinforcement. Moreover, the weak bond between the FRP bars and surrounding concrete resulted in a relatively sharp degradation curve before reaching the ultimate strength. For instance, the ductility indices SI, $K4$, and μ_u of specimen CSF-2.8%-IS-D10 were 0.97, 1.3, and 0.96 times the corresponding values of specimen CS-2%, respectively. Reviewing the ductility indices of specimens CSF-2.8%-IS-D10-J (which had smooth FRP bars) and CSF-2.8%-IR-D10-J (which had roughened FRP bars) indicated that the ductility behaviors of the two columns were quite different. Whereas column CSF-2.8%-IS-D10-J had ductility indices SI, $K4$, and μ_u of 2.1, 1.4, and 9.9, respectively, the corresponding values of column CSF-2.8%-IR-D10-J were 0, 4.14, and 12.3, respectively. This indicates the benefit of roughening the FRP bars to enhance the ultimate ductility of the column (i.e., a 25% increase in μ_u); however, the column suddenly failed upon reaching its peak strength as a result of FRP rupture. Regarding the effect of the location of the FRP bars on the ductility measurements, the results showed that placing the FRP bars in the concrete covers instead of in the concrete core caused the column to begin to degrade once it achieved its peak strength, without showing stability under the peak load. Moreover, the column could reach its ultimate strength at a greater displacement ductility through a smoother degradation manner. This was clearly observed in the behavior of column CSF-2.8%-ES-D10-J compared with column CSF-2.8%-IS-D10-J, where the ductility indices $K4$ and μ_u of column CSF-2.8%-ES-D10-J were 0.5 and 1.4 times those of column CSF-2.8%-IS-D10-J, respectively. The reason for this might be attributed to the increase in the accumulated stresses in the FRP bars when they were installed at a larger effective depth, which in turn causes an increase in the bond stresses between the FRP bars and concrete. Reinforcing the column with 8-mm-diameter FRP bars (column CSF-2.8%-ES-D8-J) caused sudden drops in the lateral strength, similar to the case in the specimen reinforced with roughened FRP bars (column CSF-2.8%-IR-D10-J). However, the degradation curve was gradual as a result of using three 8-mm-diameter bars that ruptured at two different drift levels. Although columns CSF-2.8%-ES-D8-J and CSF-2.8%-ES-D10-J share the same ultimate ductility factor, the degradation stiffness factor, $K4$, of column CSF-2.8%-ES-D8-J was nearly three times that of column CSF-2.8%-ES-D10-J. Thus, more experimental investigations on the effect of the bar surface texture (bond conditions) on the ductility indices, particularly the degradation

behavior of columns reinforced with steel and FRP bars, are required.

Residual Displacement

Residual displacement was defined as the displacement of zero-crossing at unloading on the hysteresis loop from the maximum displacement (Fahmy et al. 2010b). In this study, the residual displacements for the first cycle of each imposed lateral displacement level were determined for all tested specimens (ElGawady and Sha'lan 2011). Thus, the drift ratio versus normalized residual displacement of all tested columns was drawn as shown in Fig. 11. The normalized residual displacement was defined as the ratio of the residual displacement of each column at a drift level to that of the control column at the same drift level (i.e., $r = \delta_r/\delta_{rC}$). As the value of r for a column decreases, the column becomes more recoverable and reparable. Fig. 11 illustrates that although the value of r up to a drift of 1.7% (onset of FRP participation) was less than one for all columns, no clear stable trend could be observed. Starting from this drift ratio, a stable trend for the value of r could be observed. As expected, wrapping the plastic hinge region using an FRP jacket, as in column CS-2%-J, could not control the residual displacement of the column, where the value of r ranged from 0.95 to 1.02 up to a drift of 8%, at which the control column failed. In contrast, reinforcing the columns with FRP bars clearly decreased the residual displacement. For instance, the average value of the normalized residual displacement of columns CSF-2.8%-IS-D10, CSF-2.8%-IS-D10-J, and CSF-2.8%-ES-D10-J, reinforced with FRP bars having smooth surface textures, was approximately 0.8. The columns maintained this normalized value up to a drift level just before entering the degradation zone of each column as a result of bond failure. Following this drift level, the FRP bars could not continue controlling the residual displacement until the end of the tests. In contrast, the impact on the residual displacement became more considerable when enhancing the bond between the FRP bars and surrounding concrete. This trend can be observed in column CSF-2.8%-IR-D10-J (which had FRP bars with a rough texture) and column CSF-2.8%-ES-D8-J (which had FRP bars with a smaller diameter), in which both columns had an average value of $r = 0.7$. The columns continued controlling the residual displacement with nearly the same value of r until the FRP bars ruptured, at which the FRP bars lost their role in controlling the column performance. As a concluding remark, among all of the tested columns, CSF-2.8%-ES-D8-J had the best seismic performance in terms of the smallest residual displacement. This performance was caused by the high postyield stiffness, in the plastic zone.

Dissipated Energy and Damping Ratio

In recent decades, two indices have been defined to describe the ability of a structure to dissipate earthquake energy and hence survive major seismic events. The first index is the cumulative dissipated energy, which is computed by summing up the areas enclosed by the hysteretic loops in the lateral load-displacement relationships of the structure up to failure. The other index is the viscous damping ratio, which reflects the damage level attained during inelastic excursions. In this section, the cumulative dissipated energy, E, for all tested specimens was recorded and plotted for each drift level to further evaluate the effectiveness of the proposed reinforcement and investigate the effect of each tested parameter (Fig. 12). In the same manner, the damping ratio versus the displacement ductility were calculated and plotted for all specimens (Fig. 13).

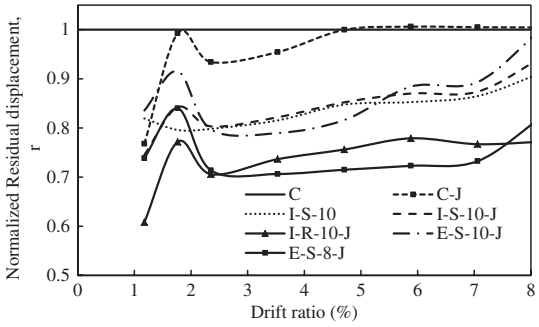

Fig. 11. Normalized residual displacement versus lateral drift ratios of the tested columns

Dissipated Energy

After calculating the energy dissipated by each loading cycle, the cumulative dissipated energy up to each drift level was determined, and the effect of each parameter was addressed (Fig. 12). Fig. 12 illustrates that the investigated parameters had only a minor impact on the cumulative dissipated energy. Up to a drift of 6%, all columns shared almost the same cumulative dissipated energy of approximately 27 kN · m. The effects of the investigated parameters were apparent beyond this drift level. After a drift of 7%, no pronounced increase in the cumulated dissipated energy was observed in the control specimen, CS-2%, as a result of the cover spalling and bar buckling that caused the failure of the specimen. By wrapping the plastic hinge with an FRP jacket, as in column CS-2%-J, the column continued dissipating more energy up to a drift of 9.4%, at which E was equal to $1.7E_C$, where E_C is the total cumulative dissipated energy of the control specimen up to failure. Then, the rate of increase was small owing to the FRP sheet bulging, which led to the failure of that column. Fig. 12 also illustrates that although adding FRP bars to the steel reinforcement caused a substantial increase in the postyield stiffness ratio, the column was able to dissipate more energy up to failure. The aforementioned observations suggest that the efficiency of reinforcing the columns with both steel and FRP bars on the amount of dissipated energy may be controlled by other variables. Thus, further investigations are still needed to determine the best configuration and best surface treatment to optimize the dissipated energy.

Equivalent Viscous Damping Ratio

The equivalent viscous damping, ζ_i, for the first cycle of all loading sets was calculated by (Jacobsen 1930)

$$\zeta_i = E_i/(4\pi E_{si}) \tag{4}$$

where E_i and E_{si} refer to the dissipated energy and elastic energy in the cycle i, respectively.

Fig. 13 shows the effect of each testing parameter on the relationship between the displacement ductility, μ, and calculated damping ratio, ζ%. Fig. 13 illustrates that up to a displacement ductility of 2, only slight differences in the damping ratio, ζ, were observed in all columns, where at this ductility, the average value of ζ was approximately 12%. There was a small decrease in the ζ for specimen CS-2%-J compared to the control specimen CS-2%, particularly after a displacement ductility of 9, at which the concrete cover of column CS-2% spalled [Fig. 13(a)]. A comparison of the results of column CSF-2.8%-IS-D10 with the control column [Fig. 13(b)] indicates that the decrease in ζ was more evident

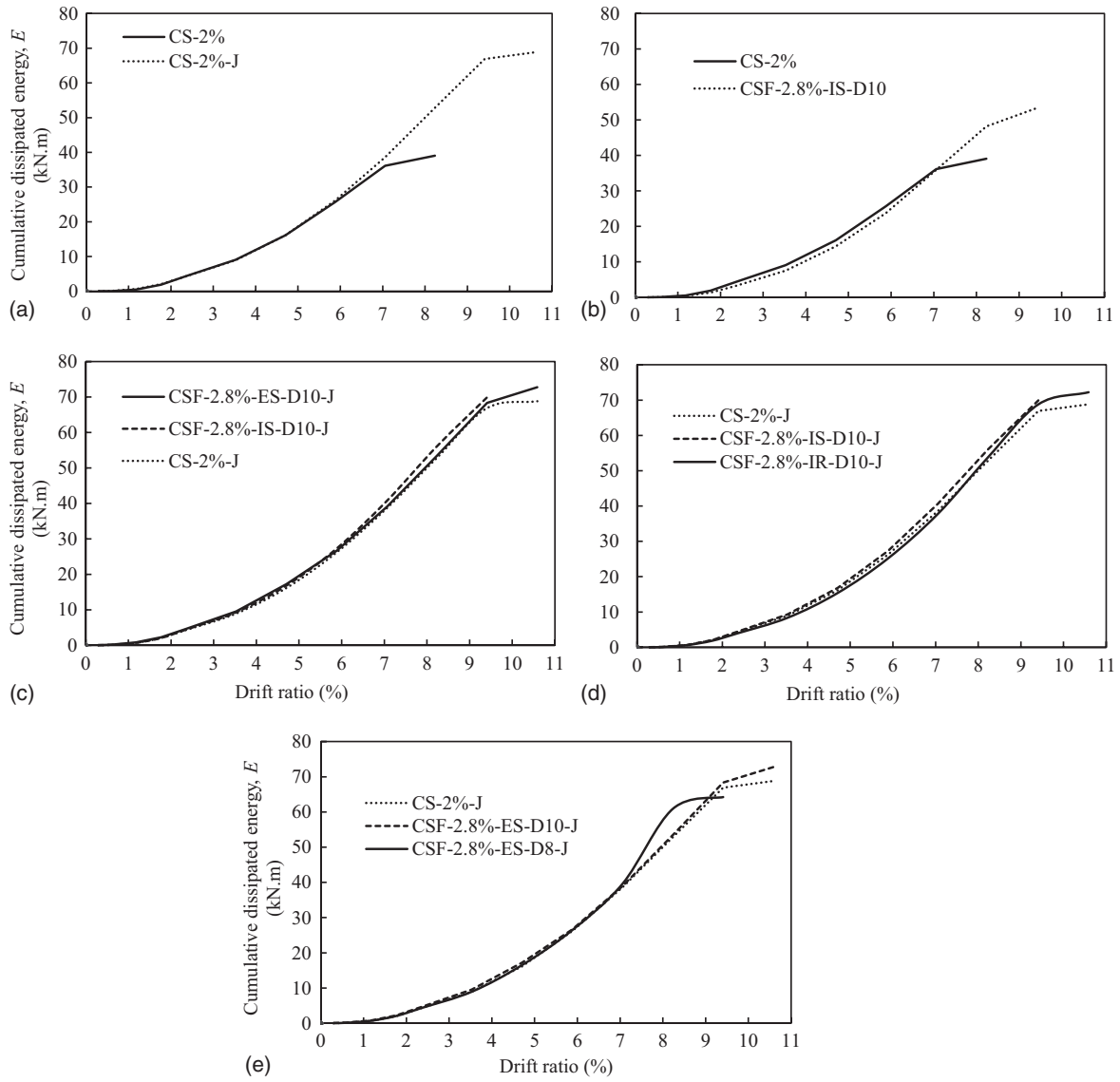

Fig. 12. Effect of all investigated parameters on the cumulative dissipated energy: (a) FRP wrapping; (b) adding FRP bars; (c) location of FRP bars; (d) FRP bar's surface configuration; (e) FRP bar's diameter

up to a displacement ductility of 9, at which both the columns started to degrade; the average loss in the value of ζ in this column was approximately 20%. Moreover, the comparison of the results of columns CSF-2.8%-IS-D10-J and CSF-2.8%-IR-D10-J with that of column CS-2%-J [Fig. 13(d)] illustrates that although reinforcing the column with internal smooth FRP bars resulted in a minor decrease in ζ up to the appearance of bond slip failure at a ductility of 8%, this decrease was more evident when using roughened FRP bars (i.e., 33% decrease). For both columns, the value of ζ approaching the failure was closer to that of specimen CS-2%-J. The average value of ζ for I-S-10-J and I-R-10-J up to failure was nearly 86 and 75% of that of specimen C-J, respectively. By placing the FRP bars externally instead of internally, as in column CSF-2.8%-ES-D10-J, the value of ζ became lower, in which the average value of ζ for specimen CSF-2.8%-ES-D10-J was almost 88% of that of specimen CSF-2.8%-IS-D10-J [Fig. 13(c)]. Finally, Fig. 13(e) illustrates that using FRP bars with 8-mm diameter caused a greater decrease in the value of ζ compared with the counterpart 10-mm-diameter BFRP bars. In other words, the decrease in the damping ratio was more pronounced when using FRP bars with a stronger bond to the surrounding concrete. This discussion demonstrates that although using FRP bars as the main reinforcement helped the column achieve higher levels of postyield stiffness without causing any loss in the column ductility and dissipated energy, the decrease in the damping ratio could be acceptable to achieve the aim of damage-controlling structures.

Which FSRC Column Could Successfully Achieve a Ductile-Recoverable Performance?

In the light of the targeted structural performance of the proposed FSRC structure, two columns could achieve the demanded ductile-recoverable performance. The first is CSF-2.8%-IR-D10-J (which had FRP bars with rough textures and was wrapped with an FRP jacket), and the second is column CSF-2.8%-ES-D8-J (which had FRP bars with a smaller diameter and was wrapped with an FRP

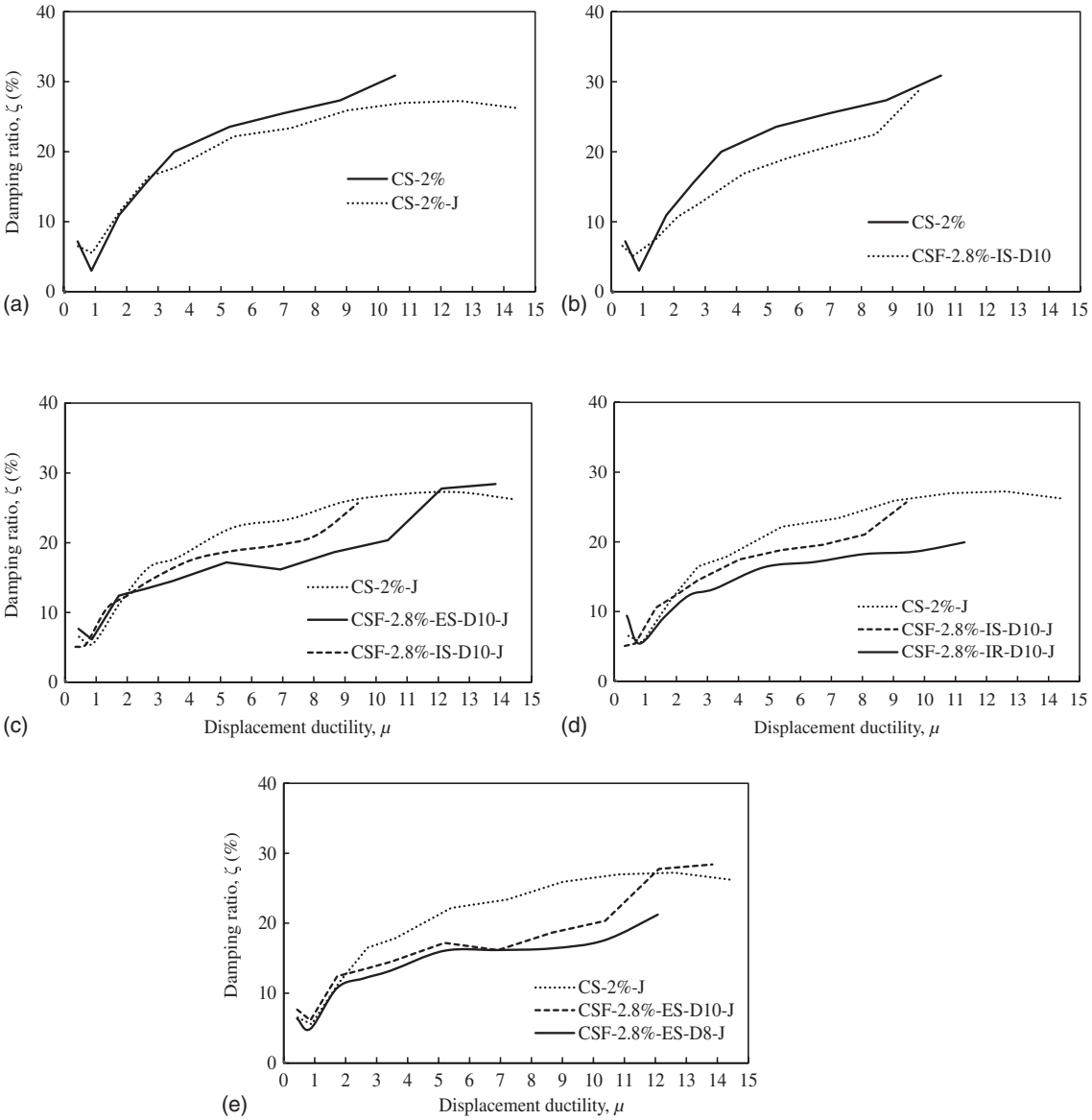

Fig. 13. Effect of all investigated parameters on the damping ratio: (a) FRP wrapping; (b) adding FRP bars; (c) location of FRP bars; (d) FRP bar's surface configuration; (e) FRP bar's diameter

jacket). Both columns had an average value for the postyield stiffness ratio of 12.6%, an average displacement ductility before load degradation of 10.85, an average ultimate ductility of 12.85, and an average residual displacement of 0.7 times that of the steel RC columns. This performance was caused by the good bonding between the FRP bars and surrounding concrete.

Summary and Conclusions

In this study, an FSRC structure was proposed as a high-seismic-performance structure. Experimental tests on the effect of constant axial load and several cyclic loadings were conducted on seven RC bridge columns, where two columns simulated the performance of SRC bridge columns and the others showed the response of the proposed FSRC columns. The roles of several bond-based parameters, such as the diameter of the FRP bars, texture of the FRP bars, location of the added FRP bars, and external confinement using an FRP jacket, were examined through the experimental program. The following conclusions could be drawn from this study:

- The proposed FRP-steel structural system ensured the existence of a stable postyield stiffness and realized the predesigned deformability capacity. With a proper design of the proposed FRP-steel reinforcement system, bridge columns could withstand a strong earthquake.
- Adding 0.8% FRP reinforcement to 2% main steel reinforcement of concrete bridge column as well as replacement of 50% of the internal steel confining the plastic hinge with external BFRP jacket guaranteed a comparable lateral strength to that of a bridge column with 4% longitudinal steel reinforcement. The FSRC column fulfilled a displacement ductility of up to 10 before encountering strength degradation.
- The elastic stiffness of the FRP steel–reinforced column was the same as that of the counterpart steel-reinforced column;

however, doubling the main reinforcement ratio of the steel-reinforced column was accompanied by a considerable increase in column elastic stiffness and a decrease in the postyield stiffness ratio.

- Within the range of the tested specimens, the average residual displacement of the proposed FSRC columns ranged from 70 to 85% that of the corresponding steel RC column. The mitigation of the residual deformations was dependent on the bond conditions between the FRP bars and the surrounding concrete. The favorable mitigation could be when BFRP bars with rough surface texture were used.
- Both the surface texture configuration and the diameter of the cross section of the FRP bars significantly influence the seismic performance and failure mode of FSRC bridge columns. Using 10-mm-diameter BFRP bars with a rough surface texture or 8-mm-diameter bars with small indentations resulted in a rupture of the BFRP bars that was accompanied by a sharp brittle failure after achieving a high strength level with reasonable ductility. Using BFRP bars with a smooth surface texture of 10-mm diameter caused lower and more stable peak strength at a smaller ductility with a smoother degradation.
- Location of BFRP bars in the column cross section with respect to the steel reinforcement had a marginal effect on both the column postyield stiffness ratio and column ductility before strength degradation. However, a considerable increase in the elastic stiffness and elimination of the stability plateau at the peak strength before strength degradation was observed when FRP bars were placed in the concrete cover rather than at the same fibers of steel reinforcement.
- Adding BFRP bars to steel RC columns maintained the cumulative dissipated energy and did not significantly decrease the damping ratio of the columns.
- Future research should be directed toward providing a better understanding of the behavior of such FRP-steel reinforcements with an emphasis on the bond condition's effect on the postpeak stability, residual displacement, and degradation stiffness. Other design parameters, including the FRP-to-steel stiffness ratio and transverse FRP reinforcement ratio, should also be examined. By monitoring the degree of damage and the condition of both steel and FRP reinforcement, the possibility of replacing FRP elements and damaged concrete to restore the original structural function is also a point of interest for future research.

References

AASHTO. (2011). *AASHTO guide specifications for LRFD seismic bridge design*, 2nd Ed., Washington, DC.

AASHTO. (2012). *AASHTO LRFD bridge design specifications*, Washington, DC.

Choi, E., Jeon, J., Cho, B., and Park, K. (2013). "External jacket of FRP wire for confining concrete and its advantages." *J. Eng. Struct.*, 56, 555–566.

Chou, C., and Chen, Y. (2006). "Cyclic tests of post-tensioned precast CFT segmental bridge columns with unbonded strands." *J. Earthquake Eng. Dyn.*, 35(2), 159–175.

Christopoulos, C., and Pampanin, S. (2004). "Towards performance-based seismic design of MDOF structures with explicit consideration of residual deformations." *ISET J. Earthquake Technol.*, 41(1), 53–73.

Christopoulos, C., Pampanin, S., and Priestley, M. J. (2003). "Performance-based seismic response of frame structures including residual deformations. Part I: Single-degree of freedom systems." *J. Earthquake Eng.*, 7 (1), 97–118.

CSA (Canadian Standards Association). (2012). "Design and construction of building structures with fibre-reinforced polymers." *CAN/CSA S806-12*, Mississauga, ON, Canada.

Currie, M. C., Rouse, J. M., and Klaiber, F. W. (2007). "Self-centering bridge piers with structural fuses." *Proc., Mid-Continent Transportation Research Symp.*, Iowa State Univ., Ames, IA.

Davis, P. M., Janes, T. M., Eberhard, M. O., and Stanton, J. F. (2012). "Unbonded pre-tensioned columns for bridges in seismic regions." *PEER Rep. 2012/04*, Pacific Earthquake Engineering Research Center, Univ. of California, Berkeley, CA.

Dawood, H., ElGawady, M., and Hewes, J. (2012). "Behavior of segmental precast posttensioned bridge piers under lateral loads." *J. Bridge Eng.*, 10.1061/(ASCE)BE.1943-5592.0000252, 735–746.

Desroches, R., and Smith, B. (2003). "Shape memory alloys in seismic resistant design and retrofit: A critical review of their potential and limitations." *J. Earthquake Eng.*, 7(3), 1–15.

ElGawady, M., Booker, A., and Dawood, H. (2010). "Seismic behavior of post-tensioned concrete filled fiber tubes." *J. Compos. Constr.*, 10 .1061/(ASCE)CC.1943-5614.0000107, 616–628.

ElGawady, M., and Sha'lan, A. (2011). "Seismic behavior of self-centering precast segmental bridge bents." *J. Bridge Eng.*, 10.1061/(ASCE)BE .1943-5592.0000174, 328–339.

El Refai, A., Ammar, M., and Masmoudi, R. (2015). "Bond performance of basalt fiber-reinforced polymer bars to concrete." *J. Compos. Constr.*, 10.1061/(ASCE)CC.1943-5614.0000487, 04014050.

Fahmy, M. F. M., Wu, Z. S., and Wu, G. (2009). "Seismic performance assessment of damage controlled FRP-retrofitted RC bridge columns using residual deformations." *J. Compos. Constr.*, 10.1061/(ASCE) CC.1943-5614.0000046, 498–513.

Fahmy, M. F. M., Wu, Z. S., and Wu, G. (2010a). "Post-earthquake recoverability of existing RC bridge piers retrofitted with FRP composites." *J. Constr. Building Mater.*, 24(6), 980–998.

Fahmy, M. F. M., Wu, Z. S., Wu, G., and Sun, Z. (2010b). "Post-yield stiffnesses and residual deformations of RC bridge columns reinforced with ordinary rebars and steel fiber composite bars." *J. Eng. Struct.*, 32(9), 2969–2983.

Hamad, B., Rteil, A., and Soudki, K. (2004). "Bond strength of tension lap splices in high-strength concrete beams strengthened with glass fiber reinforced polymer wraps." *J. Compos. Constr.*, 10.1061/(ASCE) 1090-0268(2004)8:1(14), 14–21.

Haroun, M. A., and Elsanadedy, H. M. (2005). "Behavior of cyclically loaded squat reinforced concrete bridge columns upgraded with advanced composite-material jackets." *J Bridge Eng.*, 10.1061/(ASCE) 1084-0702(2005)10:6(741), 741–748.

Iemura, H., Takahashi, Y., and Sogabe, N. (2006). "Two-level seismic design method using post-yield stiffness and its application to unbonded bar reinforced concrete piers." *Struct. Eng./Earthquake Eng.*, 23(1), 109s–116s.

Jacobsen, L. S. (1930). "Steady forced vibrations as influenced by damping." *Trans. ASME*, 50, 169–181.

Kawashima, K., MacRae, G. A., Hoshikuma, J., and Nagaya, K. (1998). "Residual displacement response spectrum." *J. Struct. Eng.*, 10.1061/ (ASCE)0733-9445(1998)124:5(523), 523–530.

Marriott, D., Pampanin, S., and Palermo, A. (2009). "Quasi-static and pseudo-dynamic testing of unbonded post-tensioned rocking bridge piers with external replaceable dissipaters." *J. Earthquake Eng. Struct. Dyn.*, 38(3), 331–354.

Mazzoni, S., McKenne, F., Scott, M. H., and Fenves, G. L. (2009). "Open system for earthquake engineering simulation user manual, version 2.0." Pacific Earthquake Engineering Center, Univ. of California, Berkeley, CA.

Nikbakht, E., Rashid, K. A., Hejazi, F., Osman, S. A., and Mohseni, I. (2013). "Seismic performance of self-centring precast post-tensioned bridge columns with SMA bars." *IJACSE*, 1(1), 24–27.

NZSEE (New Zealand Society for Earthquake Engineering). (2006). *Assessment and improvement of the structural performance of buildings in earthquakes, NZS 3101*, Wellington, New Zealand.

Palmieri, A., Matthys, S., and Tierens, M. (2009). *Basalt fibers: Mechanical properties and applications for concrete structures*, Taylor & Francis Group, London, 165–169.

Park, R. (1996). "An analysis of the failure of the columns of a 600 metre length of the Hanshin elevated expressway during the great Hanshin

earthquake of 17 January 1955." *Bull. New Zeland National Soc. Earthquake Eng.*, 29(2), 73–82.
Park, R., and Paulay, T. (1975). *Reinforced concrete structures*, Wiley, New York.
Paulay, T., and Priestley, M. J. N. (1992). *Seismic design of reinforced concrete and masonry buildings*, Wiley, New York.
Pettinga, D., Christopoulos, C., Pampanin, S., and Priestley, N. (2007). "Effectiveness of simple approaches in mitigating residual deformations in buildings." *Earthquake Eng. Struct. Dyn.*, 36(12), 1763–1783.
Priestley, M., Seible, F., and Calvi, G. M. (1996). *Seismic design and retrofit of bridges*, Wiley, New York.
Saiidi, M., and Wang, H. (2006). "An exploratory study of seismic response of concrete columns with shape memory alloys reinforcement." *ACI Struct. J.*, 103(3), 436–443.
Saiidi, M. S., O'Brien, M., and Zadeh, M. S. (2009). "Cyclic response of concrete bridge columns using super elastic nitinol and bendable concrete." *ACI Struct J.*, 106(1), 69–77.
Sakai, J., Jeong, H., and Mahin, S. A. (2006). "Reinforced concrete bridge 1175 columns that re-center following earthquakes." *Proc., 8th National Conf. on Earthquake Engineering*, EERI, San Francisco.
Seible, F., Priestley, M., Hegemier, G., and Innamorato, D. (1997). "Seismic retrofit of RC columns with continuous carbon fiber jackets." *J. Compos. Constr.*, 10.1061/(ASCE)1090-0268(1997)1:2(52), 52–62.
Seible, F., Priestley, M. J. N., and Chai, Y. H. (1995). "Earthquake retrofit of bridge columns with continuous carbon fiber jackets." *Advanced Composites Technology Transfer Consortium, Rep. No. ACTT-95/08*, Univ. of California at San Diego, La Jolla, CA.
Sheikh, S. A., and Khoury, S. S. (1997). "A Performance-based approach for the design of confining steel in tied columns." *ACI Struct. J.*, 94(4), 421–431.
Sheikh, S. A., and Li, Y. (2007). "Design of FRP confinement for square concrete columns." *J. Eng. Struct.*, 29(6), 1074–1083.
Sim, J., Park, C., and Moon, D. Y. (2005). "Characteristic of basalt fiber as a strengthening material for concrete structures." *Compos. Part B Eng.*, 36(6), 504–512.
Tazarv, M., and Saiidi, M. S. (2013). "Analytical studies of the seismic performance of a full-scale SMA-reinforced bridge column." *Int. J. Bridge Eng.*, 1(1), 37–50.
Trono, W., Jen, G., Panagiotou, M., Schoettler, M., and Ostertag, C. (2015). "Seismic response of a damage-resistant recentering posttensioned-HYFRC bridge column." *J. Bridge Eng.*, 10.1061/(ASCE)BE.1943-5592.0000692, 04014096.
Varela, S., and Saiidi, M. S. (2014). "Dynamic performance of novel bridge columns with superelastic CuAlMn shape memory alloy and ECC." *Int. J. Bridge Eng.*, 2(3), 29–58.
Wehbe, N. I., Saiidi, M. S., and Sanders, D. H. (1999). "Seismic performance of rectangular bridge columns with moderate confinement." *ACI Struct J.*, 96(2), 248–258.
Wu, G., Lu, Z. T., and Wu, Z. S. (2006). "Strength and ductility of concrete cylinders confined with FRP composites." *J. Constr. Build. Mater.*, 20(3), 134–148.
Wu, G., Wu, Z. S., Luo, Y. B., Sun, Z. Y., and Hu, X. Q. (2010a). "Mechanical properties of steel-FRP composite bar under uniaxial and cyclic tensile loads." *J. Mater. Civ. Eng.*, 10.1061/(ASCE)MT.1943-5533.0000110, 1056–1066.
Wu, Z., Wang, X., Iwashita, K., Sasaki, T., and Hamaguchi, Y. (2010b). "Tensile fatigue behavior of FRP and hybrid FRP sheets." *Compos. Part B Eng.*, 41(5), 396–402.
Wu, Z. S., Fahmy, M. F. M., and Wu, G. (2009). "Safety enhancement of urban structures with structural recoverability and controllability." *J. Earthquake Tsunami*, 3(3), 143–174.
Xiao, Y., Wu, H., and Martin, G. (1999). "Prefabricated composite jacketing of RC columns for enhanced shear strength." *J. Struct. Eng.*, 10.1061/(ASCE)0733-9445(1999)125:3(255), 255–264.
Zatar, W. A., and Mutsuyoshi, H. (2002). "Residual displacement of concrete bridge piers subjected to near field earthquakes." *ACI Struct. J.*, 99(6), 740–749.
Zhu, Z., Ahmad, I., and Mirmiran, A. (2006). "Seismic performance of concrete-filled frp tube columns for bridge substructure." *J. Bridge Eng.*, 10.1061/(ASCE)1084-0702(2006)11:3(359), 359–370.

Design and Practice of File Backup System Taking Advantage of Remotely Distributed Campuses

Hiroshi Noguchi
and Yasuhiro Ohtaki
Center for Information Technology,
Ibaraki University
Hitachi, Ibaraki 316-8511, Japan
Email: {noguchi, y.ohtaki}@mx.ibaraki.ac.jp

Masaru Kamada
Department of Computer
and Information Sciences,
Ibaraki University
Hitachi, Ibaraki 316-8511, Japan
Email: m.kamada@mx.ibaraki.ac.jp

***Abstract*—We present a file backup system designed for a university on the basis of its experiences with the 2011 east Japan earthquake. This system has two levels of security: (1) The web site for public relations and the e-mail systems for communications that will work continuously even in the case of commercial power failure. (2) The personal computer systems that will be down during power failure but will restart working without any loss of data as soon as the power supply is back. The former has been implemented by employing a private cloud computing platform and a public one in combination. To the latter, the same cloud-computing approach was not applicable because it causes latency and extra cost of communications in the normal time to keep the frequently accessed data in a cloud storage. Fortunately, this particular university has three campuses so far away that one may be destroyed by a single disaster but the other two will survive. Taking advantage of the remote campuses, we designed and implemented a file storage system that keeps the original copy on-premise in a campus and its backup copy in one of the other two campuses. Its operations have shown that the communication traffic among the campuses increased only by half in order to keep the data safe against natural disasters.**

***Keywords*-disaster robustness; business continuity planning; distributed data backup**

I. Introduction

The 2011 east Japan earthquake hit the north east part of Japan on March 11th including the three campuses of Ibaraki University [1] in Fig. 1. The buildings in Hitachi campus were severely damaged, in some cases, deep into their structural frameworks. Those in Mito and Ami campuses were also strongly shaken but less damaged for they were located relatively away from the epicenters.

The server computers were so firmly fixed to the basement that they did not fall. But they were shaken so badly that we thought the hard disk drives must have been destroyed. After the main electricity got back in several days, we were relieved and even surprised to know that the disks were not damaged at all. Probably the arms in the drives were already retracted in response to the preceding smaller vibrations while the huge main shakes were traveling from the distant epicenters. Even a smaller earthquake can destroy data on the disk drives if it takes place just beneath the server room. Data loss can give much more serious damages to the business of universities than the physical damages to the buildings.

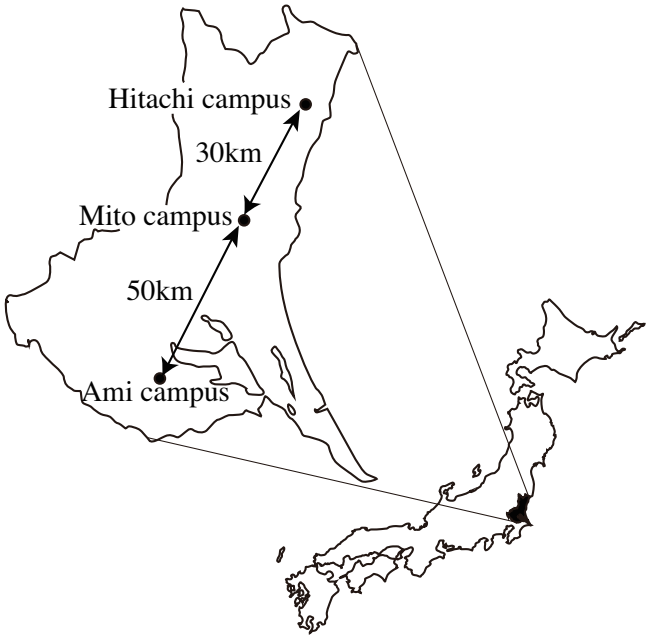

Figure 1. Three major campuses of Ibaraki University

This map shows the geographic outline of the islands and does not indicate the territory of any specific country.

It is the difficult time in disasters when we really need the means of public relation and communications. But the information systems of the university were completely out of operation for days due to the power failure. The main electricity were not available for three days in Hitachi and two days in Mito and Ami.

We really needed to announce what to do with the entrance examination scheduled on the next day of the earthquake. It was obvious that we could not do it as scheduled. But we had to announce how many days it

would be put off or if it should be cancelled. We set up an emergency web site [2] on a cloud service [3] to post announcements to the students and the employees. The temporary IP address is registered to the DNS so that the accesses to the old regular site be directed to the emergency site. This emergency site helped people get informed of the announcements from the university for a few days until the regular web site came back into operation. Then we suffered from another problem that the wrongly cached DNS records in different internet service providers kept pointing the emergency site. The heroic emergency site became a ghost web site that confused people by showing outdated information persistently.

On the basis of those bitter experiences, we have redesigned and implemented the information system of our university. This system has two levels of security: (1) The web site for public relations and the e-mail systems for communications that will work continuously even in the case of power failure. (2) The personal computer systems that will be down during power failure but will restart working without any loss of data as soon as the power supply is back.

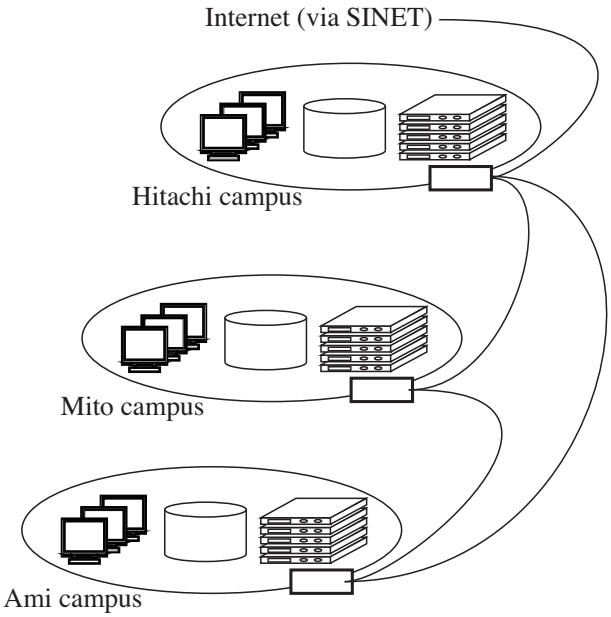

Figure 2. Network connections among the campuses.

II. Information systems and networks of Ibaraki University before the disaster

This university has three major remote campuses as shown in Fig. 1. The center for information technology is located in Hitachi campus where the computers have been historically used much more actively than the other two campuses. That is the reason why the connection to the Internet is going through the firewall system in Hitachi as shown in Fig. 2. The campuses are connected in the star-shaped topology via the wide-area ethernet at the speed of 1Gbps with the interfaces of L3 switches.

Each campus has a file server that stores the home directory of all the users in the campus. The home directory is mounted on the PC when the user logs on and also stores mails to be referred to by the mail server for the students there. The file server stores the systems and the data for the virtual servers on the real server computers managed by VMware.

The campuses have been often struck by power failure for a short time due to local thunder storms. Each campus has one of the IdP server systems so that the campus can be indifferent to power failure of other campuses. From time to time, we had power failure at Hitachi campus where the mail server for the staff and the main web servers are hosted. But the black out did not last more than half an hour.

That was strong enough against small and local disasters. But the story was different in the case of huge disaster in the wide area.

III. Lessons from mega disaster and new policy

The earthquake severely damaged Hitachi campus but fortunately claimed no casualties. We lost water supply for more than 10 days. However, in the aspect of communications, the most difficult situation was caused by the power failure for three days. The main web server and the mail server for the staff were completely down when we really needed to post announcement and discuss recovery plans to cope with the huge disaster.

The emergency web site [2] set up on a cloud service [3] was barely fulfilling the public relations. But it took some time for this new web site to start operating even though people needed information as soon as possible to know what was going on. Besides, after the regular web site came back into operation, the emergency site had suddenly become a ghost web site that confused people by showing outdated information persistently due to the wrongly cached DNS records in different internet service providers.

It is the only and best policy to keep the regular web server working throughout the disaster. The same is true of the mail servers. We have never heard of temporary mail services that can substitute existing mail services of the regular use. They are useless because we do not have a means to identify the new mail addresses of students and colleagues.

Loss of data is better than loss of lives, but it is worse than damaged buildings. It can take an enormous amount of time or may be even impossible to reproduce the lost data.

We learnt that an information system really strong against mega disasters needs the following two features:

(1) The web site for public relations and the e-mail systems for communications that will work continuously without interruption even in the case of power failure.
(2) The personal computer systems that will be down during power failure but will restart working without any loss of data as soon as the power supply is back.

The former can be implemented simply by employing the recent private or public cloud systems.

The latter requires an idea. If we employ the cloud service to keep the data safe in preparation for possible mega disasters, the data exchange between the local PC and the remote cloud causes latency and traffic in the normal time. The users should suffer from slow response of the PC due to the latency in data retrieval from the remote storage. Frequent data exchanges between the PC and the remote storage should require wide bandwidth to increase the communications cost or slow down the data transfers.

In order to store the data in a safe place while keeping the data readily accessible in the on-premise file server, we can exploit the three remotely distributed campuses connected by the 1Gbps wide-area ethernet. The local file server stores the data for the local users in each campus as it has been practiced normally. Let its duplicate copy be stored in a fellow file server in another campus. Then, at least one copy of the data will survive strong earthquakes just beneath the file server even if it would not give time to retract the disk arms.

IV. Uninterrupted Web server and Mail server

The web and mail services can be interrupted for a short time in the normal time for people usually accept regular server maintenance. On the contrary, those services should not be interrupted in the time of disaster since the latest information is crucial for the people to make decisions in emergency.

The web site can work continuously without interruption only if the server stays physically healthy and the power is uninterrupted even in the case of commercial power failure. There are roughly two kinds of solutions by means of private and public cloud systems operated at some data centers.

The main web server of Ibaraki university has been moved into a private cloud system set up in a containerized data center built in one of the campuses. It is designed to survive the strongest earthquakes in the history of Japan and supplied with main electricity by the dedicated generator. The DNS servers are extended to include the secondary DNS service hosted in a public cloud service. We are planning to move the web server further to a public cloud service.

The mail system has emigrated to the cloud service Microsoft Office 365. The IdP servers are extended to include a slave server also in a public cloud service. That is the simplest and affordable solution by virtue of the academic discount.

V. Distributed file backup system

Each campus has a file server Model VNX5300 from EMC [4] that stores the data to be preserved. They include the work space of students, electronic contents for the classes, and documents for class management. They are crucial for continuation of teaching activities through small or middle scale disasters or their quick recovery after huge disasters.

If we send the frequently updated huge data to a remote backup server outside the university in anticipation of possible mega disasters, the data transfer from the local server to the remote server causes heavy traffic in the network in the normal time. However, the fear of losing important data has been driving several Japanese universities to start a coalition to keep the data of one another [5] [6] despite the extra cost for communications and storage.

In the case of Ibaraki university where we have been suffering from the overhead cost for managing remote campuses, we have a good set of three campuses geographically apart from one another. We have only to synchronize the original copy of the data with its duplicate copy in another campus. We can keep them in the plain format without any encryption that is mandatory for the coalition of several different universities.

The backup data is a simple duplicate copy of the original one. A system image of the virtual machine and its data partition in the backup can migrate onto a different real server to start working even in the case of physical damage on the original server.

Figure 3 shows a schematic diagram of the three file servers. Each disk system is partitioned into the four regions: original copy, local duplicate copy, remote duplicate copy, and local generational archive.

The local duplicate copy is just for increasing the robustness against malfunction of the disk systems. The file server VNX5300 offers the capability of updating the local duplicate copy immediately when the original copy is modified.

The remote duplicate copy in another campus is also updated by the same mechanism except that the updates take place not immediately but every 10 minutes. This time interval of 10 minutes is a parameter that can be tuned in accordance with the real situation. A too short interval may increase the base load traffic. A too long interval may cause a burst traffic to transfer piled up updates at a time.

The local generational archive stores an ordinary incremental backup data from which users can reverse their file operation.

No data are encrypted since everything is under the control of the same institute. Nor are they even compressed. Backup data in the same plain format as the original are advantageous to save computational load for encryption and compression, and troubles for decryption and extraction in case the backup copy is needed in emergency.

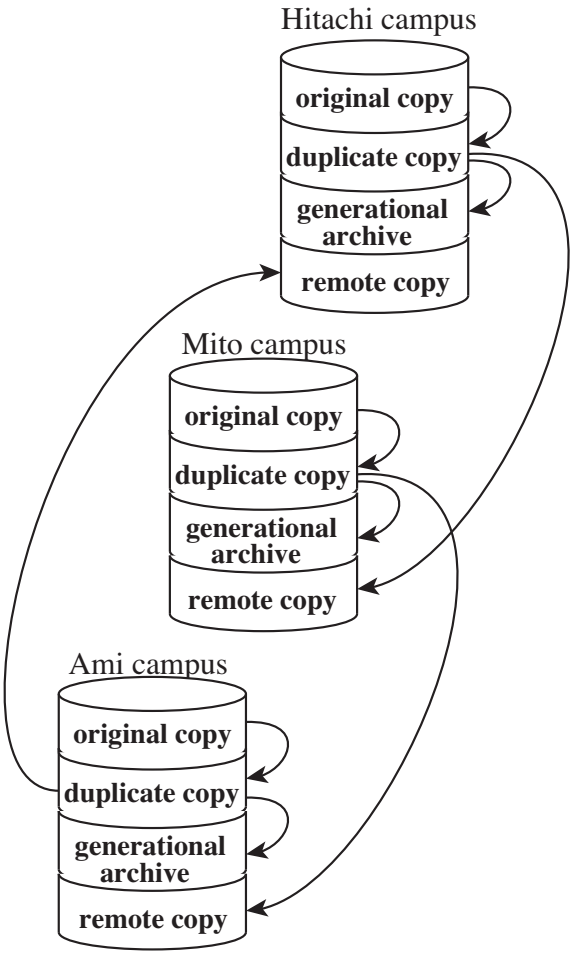

Figure 3. Structure of the copies.

VI. Evaluation

The traffic observed before and after the introduction of new backup system is plotted in Fig. 4. In the period of the measurement, the total volume of data was around 2.5T bytes. Variation from day to day of the week depends mainly on the change in the timetable of the classes.

The traffic has increased to roughly 1.5 times but stays less than 1M Bytes per second. For the wide-area ethernet connecting the campuses at the maximum speed of 1G bits per second, the new traffic rate is a moderate good figure not too low or high.

VII. Conclusions

Through the bitter experiences during the disaster in March 2011, we have redesigned the information system for Ibaraki university. The web site and e-mail systems were moved to the private and public cloud services so that they will never be interrupted again. The file servers are made

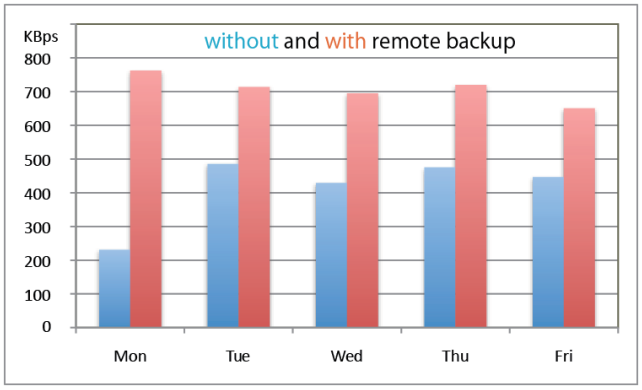

Figure 4. Averaged peak traffic of the day without (2011) and with (2012) the remote backup system.

secure by keeping a duplicate copy in another campus which is located more than 30 km away.

Taking advantage of the remote campuses, we designed and implemented a file storage system that keeps the original copy on-premise in a campus and its backup copy in one of the other two campuses. Its operations have shown that the communication traffic among the campuses increased only by half in order to keep the data safe against natural disasters.

References

[1] Ibaraki University, http://www.ibaraki.ac.jp/

[2] VIOPS Virtualized Infrastructure Operators group, http://www.viops.jp/2011/03/post-12.html, March 2011.

[3] Cloudpack, http://cloudpack.jp/

[4] EMC VNX5300, http://www.emc-storage.co.uk/emc-vnx-5300-emc-vnx5300-vnx5300-storage

[5] K. Nishimura: Implementation and evaluation of secure out-sourcing scheme for cloud storage services using secret sharing scheme, The 8th International Workshop on Security (IWSEC 2013), November 2013.

[6] Y. Kumagai et al.: A distributed file management system based on identity federation, *IPSJ Technical Report*, Internet and Operation Technology(IOT), Vol.2012-IOT-18, No.8, June 2012.

[7] M. Iwano et al.: Demonstration of non-stop backup system for business continuity plan, *IEICE Technical Report*, Vol.112, No.22, 111-116, May 2012.

沿岸域学会誌, Vol.28 No.3, pp.73－82
(Journal of Coastal Zone Studies)

2015 年 12 月

論　文

EOS-Terra/ASTERを用いた マングローブ域抽出に関する研究 —ミャンマー沿岸域を対象として—

A Study on extraction of mangrove area in Myanmar coastal zone by using EOS-Terra/ASTER —Focused on the Myanmar coastal zone—

山崎　正稔*・石内　鉄平**・桑原　祐史***
Masatoshi YAMAZAKI and Teppei ISHIUCHI and Yuji KUWAHARA

要旨：近年，地球温暖化による海面上昇，高潮，台風やサイクロンによる被害の増加が懸念されている．これらの影響による災害の減災を目的とした適応策としてマングローブが注目されているが，過伐採や植林などにより急速な分布域の変化が問題となっている．モニタリングによって分布域変化の把握が課題となっているが，分布域の広域性や多様な生物が生育する潮間帯に生育するため，急速な変化を広域に渡り捉えることの難しさが問題となっている．本研究では，この問題点と水分量に対して特長的な反応をする短波長赤外の衛星データに着目し，桑原ら（2010）の手法で課題とされていた沿岸域の地形特性（山地等）への対応とその適応効果について考察した．結論として，メコンデルタなどを対象とした桑原らの手法を改良し，沿岸域の山地に対応したマングローブ域抽出手順を提案，その適用効果を検証し，新たな手順を提案した．

キーワード：マングローブ，潮間帯，可視近赤外，短波長赤外，EOS-Terra/ASTER

1.　序論

1.1　研究の背景

近年，地球温暖化による海面上昇，高潮，台風やサイクロンによる被害の増加が懸念されている．ミャンマー連邦共和国（以下，ミャンマーと表記する）では，平成 20 年 5 月，サイクロン・ナルギスにより多くの死傷者や被害が出た [1]．その原因のひとつが防風・防波の役割を果たしていたマングローブ林の激減である [2]．マングローブは，近隣に生活する人々に生活に欠かせない様々な恵みを提供してきた [3]．また，マングローブ林は海水と淡水の入り混じる環境で生育することから，強風や高潮から海岸線を守る海岸防災林の役割を持ち，水産資源の涵養の場としての機能も備わっている．また，資金調達が難しい発展途上国にとって，自然物であるマングローブは防波堤建設などに比べ，コスト面でも安価であり有効的な海岸保護や侵食対策になりえる．ミャンマー環境保全森林省では技術者の育成を進め，洪水農業に加え，マングローブ等を指標とした環境問題への取り組みに対する衛星利用の重要性を認識している [2]．また，現在行われているマングローブ分布域を確

*　学生会員 茨城大学大学院 理工学研究科 都市システム工学専攻，**　明石工業高等専門学校 都市システム工学科
***　正会員 茨城大学 広域水圏環境科学教育研究センター

認する手段として，マングローブアトラスによる確認，各種被覆情報などの地理情報，さらに，衛星利用の三つが主である．このような中，マングローブ分布域作成を目的とした場合，広域性・同時性・周期性に優れた衛星データの利用が有効である．既往研究における報告では，LANDSAT/TMの短波長赤外バンドを利用し陸域植生の区分を行った後，マングローブ樹種の区分に対し近赤外と短波長赤外バンドを用いることが有効であるとの報告がある[4)5)]．また，ASTERデータを用い，NDVI（正規化植生指標）から植物の活性度の高い領域を抽出し，可視近赤外の各バンドの値（DN：Digital Number，以下，DN値とする）から分布を検討した例もある[4)]．以上を統合すると，衛星利用に注目が集まるなか，将来的に全球を対象として，高い更新頻度に即した簡易なマングローブ域の抽出法の提案が望まれている．

1.2 研究の目的

本研究では，気候変動による海面上昇や高潮，台風，サイクロンによる被害を推定し，適応策提案に結びつけるために必要な地理情報として，衛星データからミャンマー沿岸部のマングローブ分布域を作成することを目的とした．その際に，マングローブ分布域の作成方法は，桑原らの方法を基本とした．ミャンマー西部沿岸域では低地と山地が隣接し混在する特徴がある．したがって，地形を考慮に入れた手順の改良を行うことで他地域への汎用性を検討することにした．具体的には，ミャンマーの地域性を考慮した潮間帯の抽出方法の改良とおよび低地と山地が混在する沿岸域の対応を工夫することを目的とした．以上の目的を踏まえた研究の流れを図-1に示す．

1.3 研究対象地域

研究対象地域は，ミャンマーにおいてマングローブの植生が見られるとされるイーヤワディ川デルタ地帯(以下，イーヤワディデルタと表記する)とする．イーヤワディデルタのマングローブ分布図が現存する．マングローブアトラス(2010)を図-2に示す[6)]．この図を，衛星データからの抽出結果の良否を判断する基準データとした．

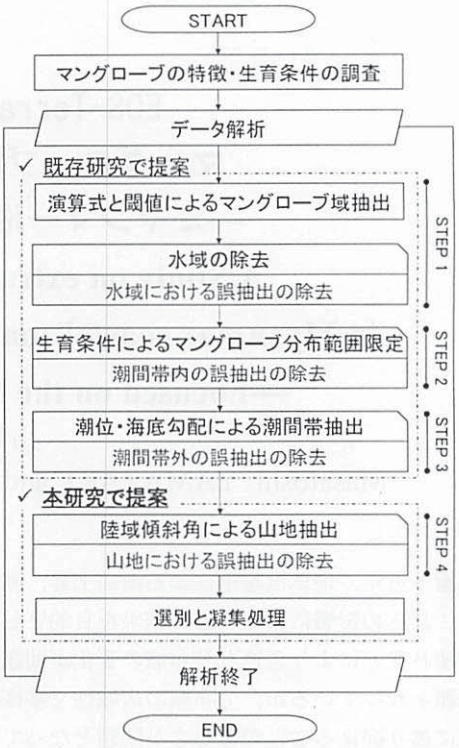

図-1 研究の流れ

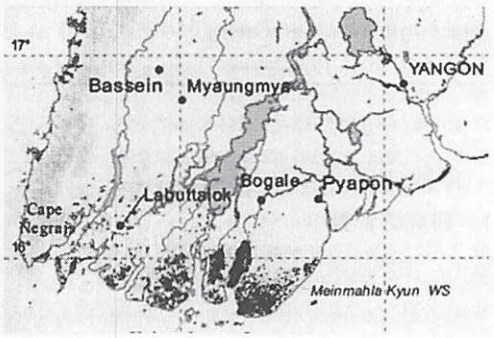

図-2 イーヤワディデルタのマングローブ分布[6)]

2. 研究方法

2.1 衛星データ

本研究では解析データとして ASTER データを使用する．ASTER は EOS-Terra 衛星に搭載されている光学センサである．解像度はバンドによって異なるが，高解像度のものは 15m であり，本論でのマングローブ域の精度は約 1/50,000 程度の縮尺を目途として議論し，広範囲に生育するマングローブ林などの抽出や解析への対応を目指す．また，マングローブのような蒸発散量の多い地物の抽出に適する短波長赤外（SW）を計測している点に注目した．ただし，ASTER はセンサ故障のため，現在,SW の計測はされていないが，2014 年 8 月に打上げに成功した WorldView-3 では，解像度約 4m と ASTER より高い空間分解能での SW 観測が開始されているため，本研究の成果はそちらのデータを用いた研究への応用展開も望める．表-1 に使用データの一覧を示す．ASTER データの取得時期は，雲の影響を考慮し，乾季とされる 10 月中旬から 2 月中旬を中心に 7 時期のデータを用いた．

表-1 EOS-Terra/ASTER データ諸元

No.	撮影日	分解能	レベル	雲量(%)
1	2002/1/4	15～30m	1B	1
2				10
3	2002/12/22			1
4				1
5	2003/1/23			14
6	2004/1/17			1
7	2004/1/19			3
8	2004/3/5			1
9				1
10	2004/12/20			1
11				1

2.2 使用データ（地理情報）

陸域地形データとして SRTM[7]，水深データとして ETOPO1[8]，時間毎の潮位データとして UHSLC hourlydata[9]，海岸線マスクデータとして SWBD[10] を使用した．GIS データである SRTM, ETOPO1, SWBD の比較を表-2 に示す．これらのデータと ASTER データの各分解能の違いについて，オーバーレイした後に出力するデータを 90m として解像度を統一することとした．

表-2 各 GIS データ比較

名前	形式	仕様	分解能
SRTM	ラスタ	陸域標高	90m
ETOPO1	ベクタ	海域標高	約2km
SWBD	ベクタ	海岸線マスク	なし※

※SWBD はベクタ形式のため解像度なし

3. ASTER 画像からのマングローブ域抽出

3.1 NDVI の算出

NDVI とは，マルチバンドデータから求められる植生の有無・多少・活性度を示す指標のひとつである．ASTER データより算出した対象地域の NDVI から耕作地とマングローブ域，それぞれ 5 箇所ずつをトレーニングエリアとして選定し，NDVI を利用してマングローブ域の抽出が可能か検証した．各被覆の指標値の分布を表-3 に示す．表-3 より，マングローブ域周辺に分布する耕作地とマングローブ域の指標値は類似した値であり，値の分布が被覆間で重複しているため，NDVI のみによってマングローブ域を抽出することは困難であり，抽出プロセスに工夫が必要であることが確認された．

表-3 各被覆における NDVI

	最小値	最大値	平均値
耕作地	-0.415	0.441	0.049
マングローブ	0.068	0.583	0.454

3.2 分布域抽出生成の考え方

NDVI のみを利用した方法では，マングローブ

$$C_n = \frac{B3 - \frac{1}{3}\sum_{n=5}^{7} n}{B3 + \frac{1}{3}\sum_{n=5}^{7} n} \quad \cdots (1)$$

B3：バンド3　n：バンド5・6・7

(C_nは-1～+1の値をとり，+1に近いほどマングローブの分布密度や活性度が高いことを示す)

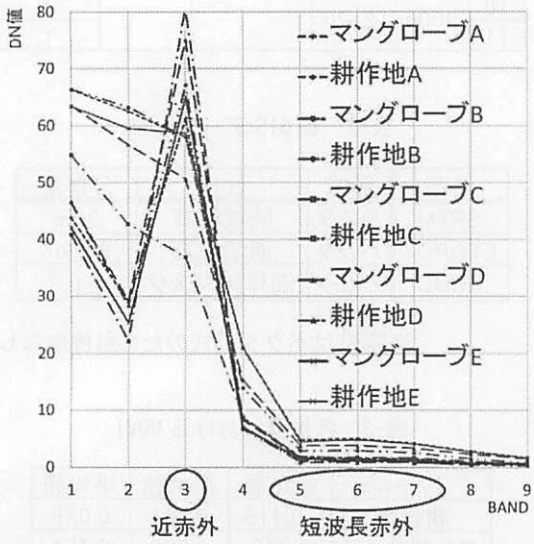

図-3 耕作地とマングローブにおける各バンドのDN値平均

表-4　設定したASTER閾値

No.	撮影日	閾値	
		最小	最大
1	2002/1/4	0.936	0.976
2			
3	2002/12/22	0.951	0.980
4			
5	2003/1/23	0.921	0.951
6	2004/1/17	0.926	0.959
7	2004/1/19	0.923	0.956
8	2004/3/5	0.931	0.965
9			
10	2004/12/20	0.936	0.976
11			

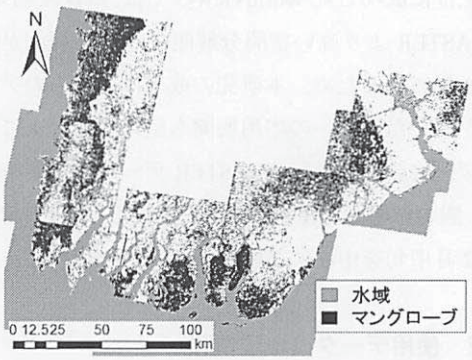

図-4 演算式による抽出処理と水域除去処理の結果（図-2中 STEP1）

域を抽出することが困難であるため，桑原らによって，メコンデルタ等を対象に提案された指標，マングローブ抽出指標 C_n（式(1)）を利用した．事前に，マングローブ域と耕作地の地表面反射率を比較した結果，両者の反射率に大きな違いがあることが確認できた．具体的には，マングローブ域と耕作地から各5地点を選出し，DN値を求めた．結果を図-3に示す．クロロフィルの影響によりマングローブ域のDN値が最も高くなるバンド3（近赤外），マングローブの蒸発散に反応しマングローブ域と耕作地が安定して分類でき，かつ，バンド3とのデータレンジ差が大きいバンド5・6・7（短波長赤外）を利用できることがわかる．

以上から，近赤外域と短波長赤外域のDN値を用い，式(1)に示す比演算式により計算するマングローブ抽出指標：C_nの適応がミャンマーにおいて可能であることが確認できた．

3.3　演算式によるマングローブ域の抽出と水域除去処理

水域から誤抽出を取り除くため，水域データの作成を行った．一般的に，近赤外より長波長の光は水に強く吸収される特性があるため，近赤外より長波長のセンサを用いて得られた画像では陸域と水域の区別がつきやすい．そこで，本研究では，

細かい汀線近傍の地形特徴を抽出することを考慮に入れ，短波長赤外より解像度の高い近赤外データ（15m）を用いて水域の抽出を行った．処理に関しては，潮間帯を削り過ぎずに領域を除くことができる衛星データの閾値を試行により検討し（表-4），二値化処理により水域を抽出した．水域，マングローブ域および陸域がオーバーレイされている結果を図-4 に示す（処理前：1,809,797pixel，処理後：718,335pixel）．なお，閾値はマングローブ域と他の土地被覆の境界の DN 値から取得し，ASTER データの取得時期ごとに分けて決定した．図-4 より，この処理において主として海域や湾部近傍の水域における誤抽出はほぼ除去できたが，内陸部の水田・湖沼部といった湿地部近傍にもマングローブ域が点在しており，陸域においてデータ処理での対応が必要となった．

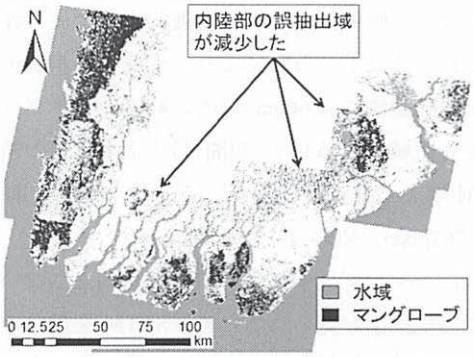

図-5 生育条件による処理を行った処理結果（図-2 中 STEP2）

図-6 潮位と海底勾配による限定法

3.4 マングローブの生育条件による分布域の検討

この処理では，マングローブの生育条件に合致しないと思われる陸域の誤抽出域の除去を目的とした．そのため，マングローブの生育域である潮間帯の特徴に注目した．潮間帯は，植生，土壌，水域が混在する．そこで，NDVI・NDWI（正規化水指標）・NDSI（正規化土壌指標）を利用し，潮間帯におけるマングローブ分布域の特性を限定した．マングローブ分布域，耕作地の土地被覆ごとに各 5 か所トレーニングエリアとしてサンプルを抽出した結果，マングローブ分布域が示す範囲は $0.25 \leqq NDVI \leqq 0.60$，$0.35 \leqq NDWI \leqq 0.70$，$-0.85 \leqq NDSI \leqq -0.50$ であった．本研究では，この条件を同時に満たす領域をマングローブ生育の条件とし，満たさない領域を削除した．抽出結果を図-5 に示す（処理前：718,335pixel，処理後：451,763pixel）．

次に，海岸線からの地形形状に注目し，潮間帯そのものを特定した．マングローブは，海水と淡水の入り混じる環境である潮間帯に生育する．そこで，海水が陸方向に浸入する限界線を推定することで抽出結果を生成できると考えた．対象地域の潮位データ（UHSLC hourlydata）から，最高潮位と ASTER データ撮影時の潮位を算出し，また，水深は ETOPO1 より算出した．その際に，図-6 に示す地形勾配法が必要となる．勾配は，沿岸に 5 本の測線を発生させ，ETOPO1 より計算した結果 0.011 度となった．ETOPO1 は約 2km メッシュの水深データであるため，推定した勾配は概略値であることは否めない．しかし，デルタ地帯の地形が平坦（内陸 100km まで標高差 5m 以内）であるため，概ね妥当と考えた．この点について分解能が約 2km の ETOPO1 を用い，境界を数値で議論することには限界があるが，海外を対象とした解析において全球を同一基準で整備したデータは

数少なく，傾斜面での解析精度向上は今後の課題としたい．以上の方法により，作成した水域データから内陸側に 4,600m 以内の範囲をマングローブ生育領域（図-6 中 *l*：潮間帯）とした．他の領域を削除した結果を図-7 に示す（処理前：451,763pixel，処理後：236,208pixel）．

次に，マングローブ生育の条件を満たさない山地にも誤抽出が見られるため，SRTM を用いて作成した陸域の傾斜角から誤抽出の除去を行う．平地と山地を区別する際の閾値は農学と建築の分野の定義から決定した．まず，農地における最大傾斜角は放牧牛が傾斜地を自由に歩行できる範囲が斜面傾斜角 6 度であるため 6～12 度である[11]．また，建築の分野においても傾斜角が 6～8 度以上になると安全性が失われ危険を伴うため，傾斜地用の基礎処理を行った後に構造物の建設を行う．よって，本研究では平地と山地の閾値を 6 度とした．傾斜角 6 度以上の誤抽出域を取り除いた結果を図-8 に示す（処理前：236,208pixel，処理後：207,566pixel）．

3.5 選別と凝集処理

本研究で使用した衛星データの分解能は 15m～90m である．このため，90m×90m の矩形領域内の被覆が混在している場合に必ずしもマングローブ域でない地点が抽出される可能性がある．このため本研究では，マングローブ域抽出を目的とした研究であることから，領域としては小さすぎる孤立した領域の除去が必要であるため，選別と凝集処理※1 を行った．凝集と選別処理により分類画像のノイズを除去することがでる．選別処理によって閾値のサイズにしたがって孤立したピクセル群を除去することができ，凝集処理によって分類後の類似性の高い隣接領域を接合して既存領域の空間的干渉性の向上が期待できる．選別の閾値を 9Pixel，凝集の閾値を 3×3Pixel とし，その処理結果を図-9 に示す．

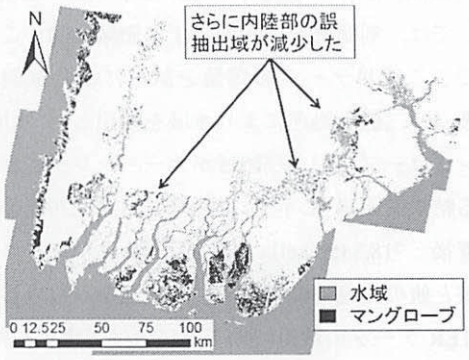

図-7 潮間帯を抽出する処理結果（図-2 中 STEP3）

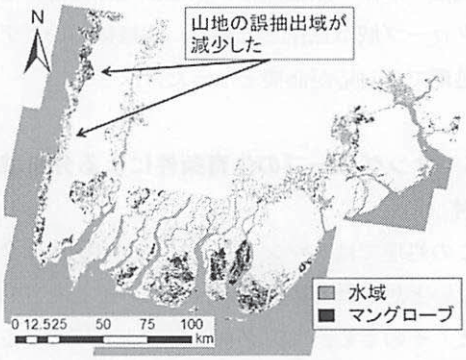

図-8 陸域傾斜角で抽出した山地を除いた処理結果（図-2 中 STEP4）

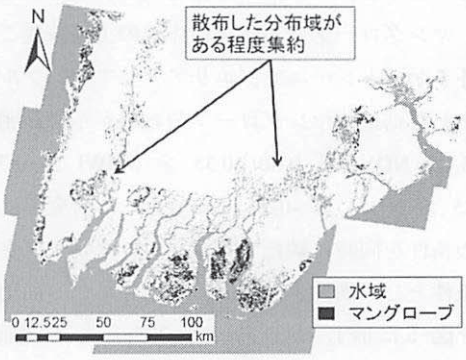

図-9 選別・凝集処理結果

3.6 抽出結果と考察

マングローブ域抽出結果（2002-2004）とマングローブアトラス(2010)，Google Earth(2013)との比較画像を図-10 に示す．また，図-10 における領域①と領域②の拡大図を図-11，図-12 に示す．データ取得時期に差異はあるが，抽出処理結果はマングローブアトラスと概ね同等の抽出結果が得られたことが分かる．しかし，山地に対して平地と同条件での抽出処理を行ったため，既存研究のメコンデルタでは確認できなかった山地における誤抽出がみられた．よって，山地に対して傾斜角を考慮に入れた抽出処理が必要となった．また，イーヤワディデルタは干満差が約 5m もあり [9]，平地では非常に平坦な土地が続くため [7]，内陸の河川まで塩水であることを条件として潮間帯を抽出し，内陸部の誤抽出域除去を行った結果，マングローブ域の抽出に精度向上が見られた．また，水域の通出や生育条件の導入，そして選別と凝集といった個別のデータ処理を組み合わせた本研究のマングローブ抽出プロセスは数値や閾値に依存するため，試行検討による最適値の導出が重要であった．

4. 結論

本研究を通して以下の三点の成果を得た．

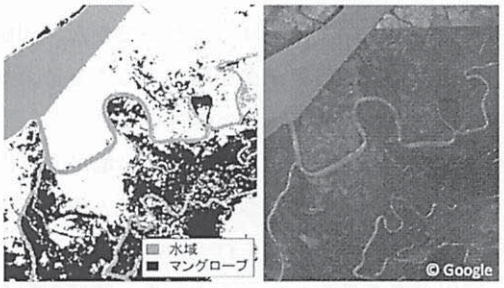

図-11 領域①における比較

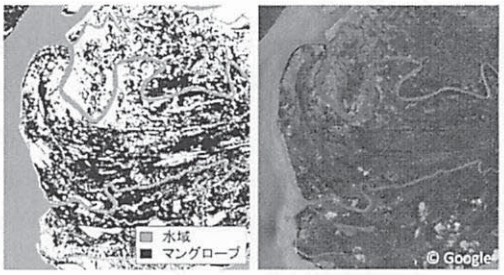

図-12 領域②における比較

図-10 マングローブ域抽出結果（上左）・マングローブアトラス（下左）・Google Earth（下右）の比較

① 式(1)で計算するマングローブ抽出指標に加え，西部沿岸域における低地と山地への処理プロセスを加えることによって，ミャンマーにおいても高精度にマングローブ域を抽出できることが確認できた．しかし，この手法は地域毎に閾値を試行検討し，最適値を導出する必要がある．この点について本研究では，空中写真や標高データ，土地利用図などを総合的に考慮し，閾値決定の方法を支援し，抽出精度の向上に繋げることができた．閾値選定を支援するデータを精査することにより適用効果と精度の向上を検討した．

② イーヤワディデルタは平地と山地が入り混じる複雑な地形を持つため，平地と山地で同じ生成法による抽出を行った場合，山地に誤抽出が多く見られた．その結果，陸域勾配を考慮し，山地の誤抽出を削除することで精度の向上が見られた．

③ イーヤワディデルタは内陸の支川部にも多くのマングローブが生育していることを考慮し，このエリアに対し，陸域の標高データと潮位から塩水となる海域エリアを，河口から内陸の河川まで探索させることで河川が内陸部まで入り組む潮間帯の変化に適応できることが確認された．

補注

※1　選別と凝集処理[19]

凝集と選別により分類画像のノイズ除去をすることができる．通常はまず，選別処理を行い閾値のサイズ（ピクセル数）に従って孤立したピクセル群を除去し，次に，凝集処理を行って分類後の類似性の高い隣接領域を結合して既存のクラスの空間的コヒーレンシーを向上させることができる．

引用・参考文献

1) ジャパン・プラットフォーム，ミャンマー・サイクロン被害者支援：http://www.japanplatform.org/programs/myanmar-cyclone/，2015.8

2) 丸紅エアロスペース株式会社：インフラ・システム輸出促進調査等（ミャンマーにおける小型衛星インフラ・システム輸出調査）調査報告書，2012.

3) 海津正倫，平井幸弘：海面上昇とアジアの海岸，2001

4) 財団法人資源環境観測解析センター：資源・環境リモートセンシング実用シリーズ⑤地球観測データの利用(2)，pp.53-67，2005.

5) Y Kotera,M Ochi,M hato : Generation of seismic base mapping using satellite image in the southern deltaic area, people's republic of Bangladesh, Proceedings of the 18th Asian Conference on Remote Sensing, 1997.

6) Mark Spalding, Mami Kainuma, Lorna Collins: World Mangrove Atlas,pp.118-121,2010

7) アメリカ地質調査所（USGS）：http://dds.cr.usgs.gov/srtm/，2015.2

8) NOAA ETOPO1 Global Relief Model，https://www.ngdc.noaa.gov/mgg/global/global.html，2015.2

9) UHSLC：http://uhslc.soest.hawaii.edu/，2015.2

10) アメリカ地質調査所（USGS）:https://dds.cr.usgs.gov/srtm/version2_1/SWBD/，2015.2

11) 井出保行，小島誠，林治雄：傾斜放牧草地の地形と草地管理：1．裸地と排糞の分布，日本草地学会誌 Vol.44(3)，pp.208-214，1998

12) 桑原祐史，田中健太：マングローブ分布域の抽出精度向上に関する研究，地球環境研究論

文集 Vol.18, pp.71-79, 2010
13) 桑原祐史, 田中健太：メコンデルタを対象としたマングローブ分布域の推定方法に関する研究, 地球環境研究論文集 Vol.17, pp.69-75, 2009
14) Mark Spalding, Francois Blasco and Colin Field : World Mangrove Atlas, pp.75, 1997
15) 大野勝弘：ミャンマー・エーヤワディーデルタにおけるマングローブ生態系の在地的管理に関する研究, 2007
16) 田村正行：短波長赤外バンドとディジタル標高 モデルによるマングローブ林の抽出, 日本リモートセンシング学会誌 Vol.32, pp.221-231, 2012
17) 竹内渉, 安岡善文：衛星リモートセンシングデータを用いた正規化植生, 土壌, 水指数の開発, 写真測量とリモートセンシング Vol.43(6), pp.7-19, 2004
18) IPCC 第5次報告書
19) EXELIS : ENVI チュートリアル マルチスペクトル分類

著者紹介

山崎　正稔（学生会員）

茨城大学大学院理工学研究科都市システム工学専攻（茨城県日立市中成沢町4-12-1), 平成3年生まれ, 平成27年3月茨城大学工学部都市システム工学科卒, 同年4月茨城大学大学院理工学研究科都市システム工学専攻入学, 土木学会学生会員.
E-mail:15nm820y@vc.ibaraki.ac.jp

石内　鉄平（非会員）

明石工業高等専門学校都市システム工学科（兵庫県明石市魚住町西岡 679-3), 2001年茨城大学工学部都市システム工学科卒業, 2003年同大学院修士課程修了, 2008年同大学院博士課程修了, 2008年博士（工学), 同年茨城大学産学官連携イノベーション創成機構非常勤研究員, 2010年明石工業高等専門学校都市システム工学科助教, 講師を経て, 2014年より同校准教授, 現在に至る. 土木学会・日本都市計画学会・日本造園学会・日本リモートセンシング学会・環境情報科学センター・日本福祉のまちづくり学会・日本測量協会、各会員.
E-mail : ishiuchi@akashi.ac.jp

桑原　祐史（正会員）

茨城大学広域水圏環境科学教育研究センター（茨城県日立市中成沢町4-12-1), 1992年東京理科大学理工学部土木工学科卒業, 1995年茨城大学工学部都市システム工学科助手, 講師, 准教授, を経て, 2015年茨城大学広域水圏環境科学教育研究センター教授(センター長), 現在に至る. 博士（工学). 日本沿岸域学会, 土木学会, 日本リモートセンシング学会, 地理情報システム学会, 環境情報科学センター, 地盤工学会, 各会員.
E-mail : yuji.kuwahara.rs@vc.ibaraki.ac.jp

A Study on extraction of mangrove area in Myanmar coastal zone by using EOS-Terra/ASTER —Focused on the Myanmar coastal zone—

Masatoshi YAMAZAKI and Teppei ISHIUCHI and Yuji KUWAHARA

ABSTRACT : The objective of this study is to propose the mangrove distribution map in Myanmar coastal zone by using satellite remote sensing data based on the estimation method of mangrove area (Kuwahara et al. 2010). Global warming and sea-level rise are projected to affect seriously on low-land area. Therefore, recently, the mangrove forest is important to decrease the damage which is received from storm surge and sea-level rise. However, because of the mangrove forest distribution area decreases, it is thought that the monitoring becomes important to confirm the area. So we adopted this method to mangrove area extraction and verified the versatility of its method.

KEYWORDS : *Mangrove, Intertidal zone, Visible and near infrared, Short wavelength infrared, EOS-Terra/ASTER*

3.プロジェクト業績

活動実績

【都市インフラの強靭化技術開発】

炭素繊維やパサルト繊維による構造補強材の高性能化により、インフラ構造物の耐震性やResilience（自己回復性）向上手法を開発し、都市インフラの強靭化技術に関する取り組みを行っており、産学連携を検討している。（呉教授）

【都市インフラモニタリングや知能化による高度化センサ技術の開発】

1）光ファイバセンサ方式とカーボンファイバセンサ方式による長寿命・高性能化された分布型領域センサの実製作・性能究明および実用性を実験室レベルで検討した。
2）領域センサにより得られるひずみ分布の直接利用により、構造物の早期損傷検知に対する各種指標を検討した。
3）開発したセンサ、装置、検知アルゴリズムを基に、早期損傷検知システムを開発し、茨城県内のRC桁橋、新潟県内の既損傷PC箱桁橋、東北新幹線高架橋、中国の蘇通大橋（１０００m級長大橋）など既設構造物のリアルタイム健全性評価システムの検証を進めている。
4）高度化された光ファイバ分布センシング技術による広域地圏環境（河川堤防・地すべり）防災システムの構築に関する産官学連携プロジェクトを開始し、基礎検討を行っている。（呉教授）

【センサデータの安定した通信/解析技術の開発と省電力化推進】

1）大規模災害により、電源インフラが完全消失した状況において、市民にどのように、情報を伝達するか、また市民の安否情報をどのように収集するかについて研究を進めている。内部電源を必要としないUHF帯RFIDを利用している。（武田教授）

【老朽化したインフラ構造物の災害リスクを考慮した維持管理計画】

1）橋梁の（異常監視）ヘルスモニタリングシステムの実証実験を常陸大宮市の引田橋での継続的に実施した。（齋藤特命教授,原田准教授，鎌田教授）

2) ひたちなか海浜鉄道湊線での企業との傾斜計の実証実験を推進．本件は 10 月に茨城県土木部常陸大宮土木事務所との連携で常陸大宮地区の地すべり危険地域へ３基設置．現在データ収集中（齋藤特命教授）
3) 構造物の耐久性設計に資する高度化シミュレーション技術を開発している（車谷准教授）

【UAV を活用した新たな空間情報の防災システムへの活用と超小型衛星との連携】

1) 茨城県生活安全部と UAV による安全監視・不法投棄防止システムの実現の連携検討を開始した。（齋藤特命教授）
2) 宮城教育大学との UAV を用いた空間環境情報可視化と津波災害地域の空撮を行った。（齋藤特命教授）
3) 宮城県石巻市、女川町での空撮による災害地域の土地利用変化、震災遺構の映像保存プロジェクトをスタートさせた。（齋藤特命教授）
4) 茨城県土木部河川課との連携で、茨城県が管理するダムの長寿命化のための映像撮影を 10 月より開始。（齋藤特命教授）

【アウトリーチとしての防災・減災、それらを含む環境教育の実施】

1) 日本リモートセンシング学会との共催で、守谷市内小学校で防災における空間情報応用に関する講演を実施した。（桑原教授）
2) ひたちなか市外野小学校、前渡小学校にて環境・情報教育を実施した。（齋藤特命教授）
3) (社)次世代センサ協議会第 44 回センサ＆アクチュエータ技術シンポジウムにて UAV と防災について講演した。（齋藤特命教授）

【災害時および平常時等における情報共有法】

1) 防災情報を配信する方法には、インターネットやＦＭ放送、拡声器などを利用する方法があるが一長一短がある。そこで追加手段の１つとして交通信号機を配信局として用いる方法を研究している。特に、光点滅（ＬＥＤのオンオフ、人間の目ではそのオンオフは感知できない）による光ワイヤレス通信の高信頼化について検討している。
2) 大規模震災では、集中制御が基となる携帯網・ワイヤレス通信網では情報共有は難しいまた、信号機等の停電により大規模な車両渋滞が生じると考えられる。その渋滞車両を積極的に通信局として利用するネットワーク網を構築する研究を進めている。ＭＡＣプロトコルとして、変形２進カウントダウン法を考案している。（羽渕裕真教授）

【地元企業・学校等との学術連携実現】

1) 湊線の鉄道運行支援システム構築について、連携研究を実現（ひたちなか海浜鉄道、福山 C）した。（齋藤特命教授，桑原教授）

【地域社会活動】

1) 齋藤　修：ひたちなか市外野小学校等における理科教育の支援の一環として、理科・環境・情報等の総合的教育を行った（2015 年 4 月～2016 年 3 月）。
2) 鎌田　賢：第 38 回全国高等学校総合文化祭「いばらき総文祭 2014」コンピュータ部門のプログラミングコンテストにおいて、予選・本選（平成 26 年 7 月 28 日（月）29 日（火））の審査委員を務めた。本選ではデモ展示も行った。

【他大学・企業・自治体連携での研究資金獲得】

1) 東北大学と共同で申請した科研費（挑戦的萌芽）「地盤中の間隙水の挙動調査」採択（東北大学風間基樹教授，茨城大学安原一哉名誉教授，鎌田賢教授）（齋藤修特命教授の企画・アレンジによる）において、地中埋め込み型の土砂内水流・水圧センサと無線モジュールを開発した。
2) シンポジウム「SICE 計測部門セミナー 都市のスマートセンシング」を企画して開催した。（齋藤特命教授）
http://rcl.it.aoyama.ac.jp/sice-sss/sice_seminar_20140917.html

【自治体との各種連絡会議推進（茨城県・日立市・ひたちなか市等）】

1) 茨城県商工労働部、土木部、企画部、生活安全部との定期情報交換（齋藤特命教授）（鎌田教授，桑原教授は随時参加）
2) 日立市土木部、生活環境部、市長、副市長との定期情報交換（齋藤特命教授）（鎌田教授，桑原教授は随時参加）
3) ひたちなか市長との情報交換会 1 回／年度（齋藤特命教授）（鎌田教授，桑原教授は随時参加）

【国際共同研究を実施（アメリカ、英国、イタリア、中国、韓国等）】

1) 科研 S-8(安原名誉教授)におけるメコン川流域とメコンデルタの気候変動影響と災害事情調査(UAV による調査を含む)に参画した。成果は 2014 年 8 月 30 日 NHK-TV　NHK スペシャルにて放映された。
2) センシング技術による地下鉄防災システムの高度化に関する共同研究を英国のケンブリッジ大学、長大橋の長寿命化に関する研究を中国の東南大学、光ファイバ技術による高速道路橋の長期モニタリングに関してアメリカＦHWA（連邦道路管理局）橋梁の長期性能検討プロジェクトチームなどと共同研究により推し進めている。（呉教授他）

【大学院生の教育】

1) ５名の社会人博士課程入学者をリクルートした 2013 年度につづき、2014 年度には 3 名の社会人博士課程入学者をリクルートした。（齋藤特命教授）センター教員の連携による指導体制を構築している。
2) 当センター所属院生を中心にして、茨城大学学生国際会議（１１月１５日１６日：水戸キャンパス）の企画・運営を行った。（呉教授、沼尾教授、鎌田教授、湊教授、桑原教授、外岡教授）
3) 羽渕研究室学部 4 年生 高柳翔太君の研究成果発表「ＬＥＤのオンオフ信号による光ワイヤレス通信の研究成果」が電子情報通信学会東京支部学生会学生奨励賞を受賞した。（全発表数数：２２９、受賞者数：２１）
4) 羽渕研究室博士前期課程 2 年生 ライ サチン君の国際会議発表「Proposal of Turbo-Coded Differential OOK for Optical IM/DD System」が RISP International Workshop on Nonlinear Circuits, Communications and Signal Processing (NCSP'15)にて Student Paper Award を受賞した。

業績一覧

【原著論文】

1) Ibrahim, A., Wu, Z., Fahmy, M., and Kamal, D, ″Experimental study on cyclic response of concrete bridge columns reinforced by steel and basalt FRP reinforcements″, ASCE Journal of Composites for Construction, ISSN: 1943-5614, 2015.
2) Ibrahim, A., Fahmy, M., Wu, Z, ″3D finite element modeling of bond-controlled behavior of steel and basalt FRP-reinforced concrete square bridge columns under lateral loading″, Composite Structures, Vol. 143, pp. 33-5220, May 2016.
3) Ibrahim, A., Fahmy, M.F.M., and Wu, Z, ″Numerical simulation on fracturing bond mechanisms of different basalt FRP bars″, Journal of Japan Society of Civil Engineers (Applied Mechanics), Vol 71, No.4 pp. 289-298, 2015.
4) M. A. Saifeldeen, N. Fouad, H. Huang, and Z.S. Wu, ″Advancement of Long gauge carbon fiber line sensors for strain measurements in structures″, Journal of Intelligent Materials systems and structures, (accepted on Jan, 11, 2016).
5) 車谷麻緒, 川瀬晴香, ″拡張ボクセル有限要素法の開発とその性能評価″,日本計算工学会論文集, Vol.2015, pp.20150011, 2015.
6) 小林賢司,車谷麻緒,岡崎慎一郎,廣瀬壮一, ″破壊力学的損傷を考慮したコンクリート中の物質移動解析手法の開発とその性能評価″,土木学会論文集A2（応用力学）, Vol.71, No.2, pp.I_161-I_170, 2015.
7) 山崎正稔,石内鉄平,桑原祐史, ″ EOS-Terra/ASTERを用いたマングローブ域抽出に関する研究―ミャンマー沿岸域を対象として―″,日本沿岸域学会誌, Vol.28, No.3, pp.73-82, 2015.
8) T. Nagayama, S. Takeda, M. Umehira, K. Kagoshima and T. Miyajima. “Improving Performance by Countering Human Body Shadowing in 60 GHz Band Wireless Systems by Using Two Transmit and Two Receive Antennas″, IEICE Trans. on Commun., vol.E99-B, no.2, pp.422-429, Feb. 2016.
9) 宮坂隆平, 武田茂樹, 鹿子嶋憲一, 梅比良正弘, ″UHF帯RFIDによる災害電子掲示板に関する検討″,土木学会論文集F3(土木情報学), 2016.(掲載決定)
10) 宮坂隆平, 武田茂樹, 鹿子嶋憲一, 梅比良正弘, ″UHF帯RFIDによる災害電子掲示板に関する検討″,土木学会, 第40回土木情報学シンポジウム, vol.40, pp.187-190, Oct. 2015.
11) Kaoru Sugita, Ken Nishimura, Tomoyuki Ishida, ″Qualitative Evaluation of Multimedia Contents for Different Media Types and Media Quality″, International Journal of Distributed Systems and Technologies (IJDST), Vol.6,Issue 3, 2015年7月.

12) Toshiya Watanabe, Naohiro Ohtsuka, Susumu Shibusawa, Masaru Kamada, Tatsuhiro Yonekura, ″Design and Development of Lower Limb Chair Exercise Support System with Depth Sensor″, Transactions on Networks and Communications, 2015年8月.

13) Tomoyuki Ishida, Tsubasa Ando, Noriki Uchida, Yoshitaka Shibata, ″Development of Zoo Guide Smartphone AR Application for Foreign Tourists Visiting Japan″, IT CoNvergence PRActice (INPRA), Vol.3, No.3, 2015年9月.

14) Sachin Rai, Yusuke Kozawa, Hiromasa Habuchi, Yuto Matsuda, ″Mitigation of the Influence of Optical Background Noise by using Turbo-Coded DOOK″, Journal of Signal Processing, 2015年11月.

15) Kazuhiro Takahagi, Tomoyuki Ishida, Akira Sakuraba, Kaoru Sugita, Noriki Uchida, Yoshitaka Shibata,″Construction of a Mega Disaster Crisis Management System″, Journal of Internet Services and Information Security (JISIS), Vol.5, No.4, 2015 年11 月.

16) Dahanayaka, G., Quarmal, S.B., Warnajith, N., Dassanayake, G., Tonooka, H., Minato, A., and Ozawa, S,″Expansion of the Remote Sensing Research on Water Environments of Asia Through KISSEL Server System″, ICT for Development, Working Paper Series, Vol. 05, No. 1, pp. 54-63 (2015)

17) Nalin Warnajith, Nguyen Cao Thang, Sataru Ozawa, Atshushi Minato,″Mobile Radiation Measuring System using Small Linux box and GPS sensor″, Int. J. Modern Engineering Research, Vol. 5 Iss.2 pp1-6,(2015)

18) G. Anne Nisha, Nalin Warnajith, Hiroshi Tsuchida, Atsushi Minato,″Wireless sensor network system for inclination measurement using spirit level″, Int. J. Modern Engineering Research, Vol. 5 Iss.3 pp1-8, (2015)

【招待講演】

1) M. A. Saifeldeen, N. Fouad, H. Huang, and Z.S. Wu, Health monitoring of bridges based on distributed long gauge carbon fiber sensors, 2nd International Conference on Bridge Testing, Monitoring & Assessment, Egypt 2015.

2) Kurumatani, M., Terada, K., Kato, J., Kyoya, T., Kashiyama, K. . “Crack propagation analysis using an isotropic damage model based on fracture mechanics for concrete”.7th Korea-Japan Workshop on Computational Mechanics, April, 2015 (Busan, Korea).

3) Kurumatani, M., Abe, S., Nemoto, Y., Soma, Y., Henmi, N.:A method for fracture simulation of reinforced concrete using a damage model based on fracture mechanics for concrete, 3rd International Workshops on Advances in Computational Mechanics, October, 2015 (Ryogoku, Japan).

【国際会議発表】

1) Ibrahim, A., Fahmy, M.F.M., and Wu, Z. Damage-controllable basalt FRP steel reinforced concrete structural system. The 12th International Symposium on Fiber Reinforced Polymers for Reinforced Concrete Structures (FRPRCS-12) & the 5th Asia-Pacific Conference on Fiber Reinforced Polymers in Structures (APFIS-2015), Nanjing, China, December, 2015.
2) M. A. Saifeldeen, N. Fouad, H. Huang, and Z.S. Wu, Health monitoring of bridges based on distributed long gauge carbon fiber sensors, 2nd International Conference on Bridge Testing, Monitoring & Assessment, Egypt 2015.
3) Kurumatani, M., Abe, S., Nemoto, Y., Soma, Y., Henmi, N. : A method for fracture simulation of concrete using an isotropic damage model, 13th US National Congress on Computational Mechanics, July, 2015 (San Diego, USA).
4) Kunimitsu Takahashi, Masaru Kamada, ″Bivariate Splines in Piecewise Constant Tension″, Proc. of the 11th International Conference on Sampling Theory and Applications (SampTA 2015), 2015年5月.
5) E. Kato, H. Katayama, M. Sakai, Y. Nakajima, T. Kimura, K. Nakau, and H. Tonooka, ″Initial checkout results of the Compact Infrared Camera (CIRC) for earth observation″, Proc. of the 36th International Symposium on Remote Sensing of Environment, 2015年5月.
6) Tshubasa Ando, Tomoyuki Ishida, Noriki Uchida, Yoshitaka Shibata, ″Digital Contents Management System based on Position Information Initiate Fusion of AR Technology and Sensor Technology″, Proc. of the Ninth International Conference on Innovative Mobile and Internet Services in Ubiquitous Computing 2015 (IMIS2015), 2015年7月.
7) Noriki Uchida, Go Hirakawa, Tomoyuki Ishida, Yoshikazu Arai, Yoshitaka Shibata, ″IEEE802.11 based Vehicle-to-Vehicle Delay Tolerant Networks for Road Surveillance System in Local Areas″, Proc. of the Ninth International Conference on Innovative Mobile and Internet Services in Ubiquitous Computing 2015 (IMIS2015), 2015年7月.
8) Shuji Ogawa, Michitoshi Niibori, Masaru Kamada, ″Web-based Location Sharing Service for a Group of People to Get Together″, Proc. of the 4th International Workshop on Web Service and Social Media (WSSM 2015), 2015年9月.
9) Kazuomi Suzuki, Michitoshi Niibori, Adnan Saleh Rashed, Shusuke Okamoto, Masaru Kamada, ″Development of IslayPub3.0 - Educational Programming Environment Based on State-Transition Diagrams″, Proc. of the 4th International Workshop on Web Service and Social Media (WSSM 2015), 2015年9月.

10) Takahiro Inui, Masaki Kohana, Shusuke Okamoto, Masaru Kamada, "A Software Framework for Internet of Things", Proc. of the 4th International Workshop on Web Service and Social Media (WSSM 2015), 2015年9月.

11) Shota Noguchi, Michitoshi Niibori, Erjing Zhou, Masaru Kamada, "Student Attendance Management System with Bluetooth Low Energy Beacon and Android Devices", Proc. of the 4th International Workshop on Web Service and Social Media (WSSM 2015), 2015年9月.

12) Xiao-Lei Li, Osamu Saitou, Erjing Zhou, Masaru Kamada, "Library Navigation System with FeliCa Cards as Landmarks", Proc. of the 4th International Workshop on Web Service and Social Media (WSSM 2015), 2015年9月.

13) Erjing Zhou, Shusuke Okamoto, Michitoshi Niibori, Masaru Kamada, Tatsuhiro Yonekura, "IslayTouch: An Educational Visual Programming Environment Based on State-Transition Diagrams that Runs on Android Devices", Proc. of the 18-th International Conference on Network-Based Information Systems (NBiS 2015), 2015年9月.

14) Hiroshi Noguchi, Yasuhiro Ohtaki, Masaru Kamada, "Design and Practice of File Backup System Taking Advantage of RemotelyDistributed Campuses", Proc. of the 4-th International Workshop on Web Services and Social Media (WSSM-2015), 2015年9月.

15) Kazuhiro Takahagi, Tomoyuki Ishida, Akira Sakuraba, Kaoru Sugita, Noriki Uchida, Yoshitaka Shibata, "Proposal of the Disaster Information Transmission Common Infrastructure System intended to Rapid Sharing of Information in a time of Mega Disaster", Proc. of the 11th International Workshop on Network-based Virtual Reality and Tele-existence (INVITE'2015), 2015年9月.

16) Akira Sakuraba, Yasuo Ebara, Tomoyuki Ishida, Yoshitaka Shibata, "A Design of Interface Device for Counter Disaster GIS on Ultra High Definition Tiled Display Environment", Proc. of the 11th International Workshop on Network-based Virtual Reality and Tele-existence (INVITE'2015), 2015年9月.

17) Satoshi Noda, Yu Ebisawa, Yasuo Ebara, Tomoyuki Ishida, Koji Hashimoto, Yoshitaka Shibata, "Application of Tiled Display Environment for High Presence Informal Communication", Proc. of the 11th International Workshop on Network-based Virtual Reality and Tele-existence (INVITE'2015), 2015年9月.

18) Shota Takayanagi, Hiromasa Habuchi, Yusuke Kozawa, "Optical-Wireless Enhanced Code-Shift-Keying with IM/DD", Proc. of the 2015 21st Asia-Pacific Conference on Communications (APCC), 2015年10月.

19) Shota Takayanagi, Hiromasa Habuchi, Yusuke Kozawa, "Indoor Optical-Wireless Code-Shift-Keying with Two-Stages Demodulation", Proc. of the 2015 IEEE 4th Global Conference on Consumer Electronics (GCCE), 2015年10月.

20) Masaya Yamazaki, Kazuhiro Takahagi, Tomoyuki Ishida, Kaoru Sugita, Noriki Uchida, Yoshitaka Shibata, ″Proposal of Information Acquisition Method utilizing CCN in a time of Large Scale Natural Disaster″, Proc. of the 5th International Workshop on Multimedia, Web and Virtual Reality Technologies and Applications (MWVRTA2015), 2015年11月.
21) Hiroshi Noguchi, Yasuhiro Ohtaki, Masaru Kamada, Masanori Itaba, Satoru Ozawa, ″Study of future strategy ICT center – Better quality of services in the case of Ibaraki University –″, Proc. of the International Symposium on ICT in Development 2015 (ISICTD2015), 2015年11月.
22) Kazuhiro Takahagi, Tomoyuki Ishida, Noriki Uchida, Yoshitaka Shibata, ″Proposal of the Common Infrastructure System for Real-Time Disaster Information Transmission″, Proc. of the 30th IEEE International Conference on Advanced Information Networking and Applications Workshops, 2016年3月.
23) Kaoru Sugita, Ken Nishimura, Tomoyuki Ishida, ″Optimizing Media Quality Parameters to Reduce Energy Consumption for Emergency Communication Service″, Proc. of the 30th IEEE International Conference on Advanced Information Networking and Applications Workshops, 2016年3月.
24) Shota Takayanagi, Hiromasa Habuchi, Yusuke Takamaru, Yusuke Kozawa, ″Data-Rate-Enhanced Optical-Wireless Code-Shift-Keying System Having Two-Stage Demodulation″, Proc. of NCSP2016, 2016年3月.
25) Mitsuru Saotome, Yusuke Kozawa, Yohtaro Umeda, Hiromasa Habuchi、″Differencial-OOK System for Underwater Visible light Communications″, Proc. of NCSP2016, 2016年3月.
26) Atsuhiro Takahashi, Hiromasa Habuchi, Yusuke Kozawa, ″Rigorous Symbol Error Rate Analysis of Hierarchical MPPM-CNK through Optical Wireless Channel″, Proc. of NCSP2016, 2016年3月.
27) Yuto Matsuda, Hiromasa Habuchi, Yusuke Kozawa, ″Impact of Improved On-Off-Keyed Turbo-code System in Optical Wireless Channel″, Proc. of NCSP2016, 2016年3月.

【学会発表（国内、国際)】

1) 鎌田和樹，渡邉俊哉，渋沢進，“深度画像センサを用いた拮抗体操支援システムの改良と評価”，情報処理学会第163回ヒューマンコンピュータインタラクション研究会，2015年5月.
2) 高橋貴大，羽渕裕真，小澤佑介，“光無線MPPM-CNKにおける競合計数器型フレーム同期法の一検討”，電子情報通信学会ＷＢＳ研究会，2015年5月.
3) 高柳翔太，羽渕裕真，“拡張擬直交M 系列を用いる光無線コードシフトキーイングの一検討”，電子情報通信学会ＷＢＳ研究会，2015年5月.

4) 松田優人，ライ サチン，小澤佑介，羽渕裕真，“光無線通信における差動符号化OOK を用いるパンクチャードターボ符号システムの一検討”，電子情報通信学会ＷＢＳ研究会，2015年5月．
5) 外岡秀行，塩澤美咲，加藤篤，加藤恵理，片山晴善，酒井理人，加藤創史，“ALOS-2/CIRCの代替校正・相互校正の初期結果”，日本リモートセンシング学会第58 回学術講演会論文集，2015年6月．
6) 田川博務，外岡秀行,“ASTER 火災検出アルゴリズムの安定化のための一手法(その２)”，日本リモートセンシング学会第58回学術講演会論文集，2015年6月．
7) 加藤篤，外岡秀行，“雲を含む熱赤外画像マッチングにおける位相限定相関法のロバスト性評価”，日本リモートセンシング学会第58 回学術講演会論文集，2015年6月．
8) 黒木幹，伊藤将司，内田智昭 ，石田智行 ，米倉達広，“情報収集ツールを活用した市民協働のインフラ維持管理システムの運用に関する研究”, 第51回土木計画学研究発表会（春大会），2015年6月．
9) 安藤翔，石田智行，“相互関連性を考慮した拡張現実型ジオメディアの研究”，電子情報通信学会第30 回サイバーワールド研究会，2015年6月．
10) 江藤拓也，羽渕裕真，橋浦康一郎，“一般化拡張プライム符号を用いるリレーネットワークの性能評価”，電子情報通信学会ＷＢＳ研究会，2015年7月．
11) 高柳翔太，羽渕裕真，小澤佑介，“2段階復調を行う光無線コードシフトキーイングの誤り率性能評価”，電子情報通信学会ソサイエティ大会 ，2015年9月．
12) 伊形俊介，村田直也，小澤佑介，楳田洋太郎，羽渕裕真，“デジタル制御型カラーシフトキーイング方式におけるターゲットカラー制御法の一検討”，電子情報通信学会ＷＢＳ研究会，2015年10月．
13) 奥村淳平，村田直也，小澤佑介，楳田洋太郎，羽渕裕真，“4色LEDを用いた一般化空間変調方式の一検討”，電子情報通信学会ＷＢＳ研究会，2015年10月．
14) 高橋貴大，羽渕裕真，小澤佑介，“競合計数器型フレーム同期法を用いる光無MPPM-CNKにおけるシンボル誤り率特性”，電子情報通信学会ＷＢＳ研究会，2015年10月．
15) 松田優人，羽渕裕真，小澤佑介，“非均一電力割当法を用いる光無線ターボ符号化DOOKの一検討”，電子情報通信学会ＷＢＳ研究会，2015年10月．
16) 野口宏，大瀧保広，鎌田賢，“オンプレミスの電子メールサーバからOffice365 への移行”，大学ICT 推進協議会2015 年度年次大会，2015年12月．
17) 森卓哉，小澤佑介，楳田洋太郎，羽渕裕真，“高速水中可視光通信のための複数色LEDを用いた畳み込み符号化OOK方式の一検討”，電子情報通信学会ワイドバンド研究会, 2015年12月．

【受賞等】

1) 車谷麻緒:2014 年度 日本計算工学会 論文奨励賞,「破壊シミュレーションのための構造要素を用いた離散体解析手法」

【競争的資金獲得】

1.採択された競争的資金等の外部資金

1) 電気通信普及財団 研究助成金,「消失通信路に耐性のある光無線ターボ符号システムに関する研究」 1,000,000 円, 2015 年度, 研究代表者: 羽渕裕真
2) 受託研究 JAXA,「地球観測用小型赤外カメラ(CIRC)に関する校正検証」、平成 27 年度, 研究代表者: 外岡秀行
3) 受託研究 宇宙システム開発利用推進機構,「ASTER 画像の信頼性・利用性の向上に関する研究」、平成 27 年度, 研究代表者: 外岡秀行.
4) 民間企業との共同研究,「スマートグラスの処理、チューニング方法等の助言」, 研究代表者: 鎌田賢
5) 民間企業との共同研究,「路面状態センシング方式と放射分光応用に関する研究」, 研究代表者: 外岡秀行
6) 民間企業との共同研究,「路面状態センシング方式と放射分光応用に関する研究」, 研究代表者: 外岡秀行
7) 地域法人との共同研究,「訪日外国人観光客を対象とした AR スマホアプリ(iOS 版)の研究開発」, 研究代表者: 石田智行
8) 地域法人との共同研究,「訪日外国人観光客を対象とした AR スマホアプリ(Android 版)の研究開発」, 研究代表者: 石田智行

2.採択された科学研究費補助金

1) 科研費 基盤 (B) (研究課題番号 15H02693)
大規模災害時の劣悪通信環境で繋がる次世代ネバー・ダイ・ネットワークとその応用
代表 柴田義孝 (岩手県立大学) 分担 石田智行 (茨城大学)
研究期間 2015 年 4 月 1 日～2018 年 3 月 31 日
研究費総額 7,150,000 円
2) 科研費 挑戦的萌芽研究 (研究課題番号 : 26630215)
課題名 地盤中の水の挙動の調査を格段に進展できるワイヤレスマルチセンサの開発への挑戦
代表 風間基樹 (東北大学) 分担 安原一哉, 鎌田賢 (茨城大学)

研究期間　2014 年 4 月 1 日～2017 年 3 月 31 日

研究費総額 4,915,000 円

3) 科研費　基盤研究（C）　（研究課題番号：26420409）

課題名　可変張力つき 2 変数スプラインの導出とその画像補間への応用

代表　鎌田賢（茨城大学）

研究期間　2014 年 4 月 1 日～2017 年 3 月 31 日

研究費総額　1,700,000 円

4) 科研費　基盤研究(C)

課題名 センサネットワークと知識ベースを用いた高齢者見守リシステムの研究

代表 澁澤 進，H26 年度澁澤分 550 千円

研究期間　2012 年 4 月 1 日～2014 年 3 月 31 日

研究費総額　4,800,000 円

5) 科研費　基盤研究(C)

課題名 ITS のための光／電波融合型通信の高度化

代表 羽渕裕真，H26 年度 1100 千円

研究期間　2012 年 4 月 1 日～2015 年 3 月 31 日 研究費総額　4,200,000 円

茨城大学重点研究

「知的で持続可能な社会基盤および防災セキュリティ技術研究創出事業」

茨城大学工学部附属防災セキュリティ技術教育研究センター

２０１５年度報告書

発行日　　平成 28 年 4 月

発行者　　茨城大学　工学部　都市システム工学科
教授　呉　智深
〒316-8511 日立市中成沢町 4-12-1
Tel: 0294-38-5179　Fax: 0294-38-5268

茨城大学重点研究
http://www.ibaraki.ac.jp/generalinfo/activity/researching/juuten/

茨城大学工学部附属教育研究センター
http://www.eng.ibaraki.ac.jp/research/centers/index.html

防災セキュリティ技術教育研究センター
http://www.ibaraki.ac.jp/research/centers/disaster/index.html